HISTONE H3K4 METHYLATION IN HIPPOCAMPAL MEMORY FORMATION AND IN ALZHEIMER'S DISEASE

by

Yuka Obayashi

B.Sc.(Hon), Simon Fraser University, 2015

A THESIS SUBMITTED IN PARTIAL FULFILLMENT OF

THE REQUIREMENTS FOR THE DEGREE OF

MASTER OF SCIENCE

in

THE FACULTY OF GRADUATE AND POSTDOCTORIAL STUDIES

(CELLL AND DEVELOPMENTAL BIOLOGY)

THE UNIVERSITY OF BRITISH COLUMBIA

(Vancouver)

August 2021

The following individuals certify that they have read, and recommend to the Faculty of Graduate and Postdoctoral Studies for acceptance, the thesis entitled:

Histone H3K4 Methylation In Hippocampal Memory Formation And In Alzheimer's Disease

submitted Yuka Obayashi in partial fulfillment of the requirements

the degree of Master of Science

in Cell and Developmental Biology

Examining Committee:

Dr. Bradford Hoffman, Cell and Developmental Biology
Supervisor

Dr. Shernaz Bamji, Cell and Developmental Biology
Supervisory Committee Member

Dr. Jason Snyder, Psychology
Supervisory Committee Member

Dr. Timothy O'Connor, Cellular and Physiological Sciences
Additional Examiner

Dr. Cal Roskelley, Cell and Developmental Biology
Additional Examiner

Abstract

Regulation of chromatin structure through posttranslational histone modifications is implicated in the induction of synaptic plasticity and memory formation. One such modification – histone H3 lysine 4 methylation (H3K4me) – has recently emerged as a key epigenetic modification necessary for consolidation of hippocampus-dependent memory. It is well-established that H3K4me levels across the genome are dynamically regulated by opposing activity of lysine methyltransferases (KMTs) and lysine demethylases (KDMs). They link dysregulation of H3K4 KMTs to neurodegenerative disorders, such as Alzheimer's disease (AD). The major group of H3K4 KMTs in mammals are the Trithorax Group (TrxG) complexes, which can promote gene expression via distinct enzymatic (methylation of H3K4) and non-enzymatic (e.g. recruitment of other co-activators) mechanisms.

In my project, I targeted the catalytic activity of TrxG complex and demonstrated that the loss of H3K4 methylation in mature hippocampal neurons leads to several intellectual abnormalities, such as the development of anxiety-like behaviour, recognition memory deficit, and impaired reversal memory with normal locomotory coordination in mice. Furthermore, I provided evidence of reduced H3K4 methylation in the hippocampus of AD by using a combination of patient samples and rodent disease model.

Collectively, these results suggest that TrxG-mediated H3K4 methylation is required for a proper formation of hippocampal memory and may help shed light on H3K4 methylation as a novel therapeutic target for the treatment and prevention of AD.

Lay Summary

Alzheimer's disease (AD) is a progressive neurodegenerative disorder affecting 50 million people worldwide. The pathophysiology of AD is characterized by abnormal accumulation of beta-amyloid and tau proteins between nerve cells. These toxic changes are thought to hinder neuronal communication in the brain, particularly in the hippocampus– the region involved in learning and memory. Indeed, memory deficit is the most common first symptom that appears in the patients with AD, but the underlying mechanism is still unknown.

I consider that the folding of genes critical for the hippocampal memory formation is involved in the pathogenesis of AD. Using a mouse model, I demonstrated that alteration in gene folding affected hippocampal neuronal activities and memory formation. Remarkably, the alteration was also observed from the AD donors. Together, these results would help extend our understanding of AD pathogenesis, which may contribute to identifying a novel therapeutic intervention against cognitive decline in AD patients.

Preface

All of the experiments described in Chapter 2 were performed by Yuka Obayashi at the British Columbia Children's Hospital Research Institute under the supervision of Dr. Brad G Hoffman. All projects were approved by the University of British Columbia's Research Ethics Board and procedures were followed with strict compliance in accordance with the guidelines provided by the Canadian Council for Animal Care (A20-0277) and Children's and Women's Research Ethics Board (H19-03624).

Table of Contents

List of Tables

List of Figures

List of Abbreviations

Ab	Amyloid beta
ACF	Animal Care Facility
AD	Alzheimer's disease
APP	Amyloid precursor protein
BCCHRI	British Columbia Children's Hospital Research Institute
DC	Dentate gyrus
Dcx	Doublecortin
dHF	dorsal hippocampus
DNMTs	DNA methyltransferases
Dpy30⊿H	*Camk2a*-Cre; $Dpy30^{flox/flox}$ knockout
*Dpy30*WT	*Camk2a*-Cre; $Dpy30^{wt/wt}$ wildtype control
E13.5	Embryonic day 13.5
EC	Entorhinal cortex
ERK	Extracellular signal-regulated kinases
ESC	Embryonic stem cell
FACs	Fluorescence-activated cell sorting
FDR	False discovery rate
GABA	Gamma-aminobutyric acid
H3K4me	Histone H3 lysine 4 methylation
H3K9me3	Trimethylation of histone H3 lysine 9
H3K27me3	Trimethylation of histone H3 lysine 27
HATS	Histone acetyltransferases

HDACs	Histone deacetylates
HPA	Hypothalamus-pituitary-adrenal
KDMs	Lysine demethylases
KMTs	Lysine methyltransferases
KO	Kock out
LS	Lateral septum
mPFC	Medial prefrontal cortex
MWM	Morris water maze
NORt	Novel object recognition test
NSCs	Neural stem cells
OF	Open field
P20	Postnatal day 20
PBS-T	PBS with 0.1% Triton-X100
PFA	Paraformaldehyde
Pol II	RNA polymerase II
PVDF	Polyvinylidene difluoride
RM	Repeated measures
SEM	Standard error of the mean
Sub	Subiculum
SVZ	Subventricular zone
tdTomato^{+}	*Rosa26-lox-STOP-lox-tdTomato*
TFs	Transcription factors
TrxG	Trithorax Group complex

vHF	Ventral hippocampus

Acknowledgements

I would like to thank my supervisor Dr. Brad G. Hoffman for his support, advice and guidance throughout my years as a student in his lab. Thank you for always challenging me to grow and for giving me the opportunity to explore my research ideas. I would also like to thank *Cell* program director, Dr. Cal Roskelley, for taking time out of your busy schedule to discuss my research and encourage me in my future endeavours.

Further, I would like to thank my committee members, Dr. Jason Snyder and Dr. Shernaz Bamji for their technical feedback and support throughout my studies.

A big thank you to Dr. Timothy P. O'Leary for collaborating with me on this project. I could not complete the behavioural studies without his continuous support and his invaluable insights into research.

My sincerest thanks to all my lab members of Hoffman lab; former members (Dr. Stephanie Campbell and Dr. Nina Maeshima) and current members (Ben Vanderkruk and Jocelyn Bégin). They are amazing coworkers and friends who gave me enormous support throughout the last years.

I would also like to thank my best UBC buddies, Alex Kadhim, Shannon Sproul, and Meilin An, for always being on my side. I cannot imagine myself surviving through difficult years without you.

Lastly, and most importantly, thank you very much to my family in Japan and love of my life, Alex Kwok on Cheung, for unconditional love and support. Thank you for believing in me in everything I do. I love you.

Chapter 1: Introduction

1.1 The hippocampus

1.1.1 The hippocampal formation and neural connections

The hippocampal formation is a dorsoventrally elongated structure located in the medial temporal lobe of the brain. It can be divided in several subregions, including the entorhinal cortex (EC), dentate gyrus (DG), the subiculum (Sub), and the Cornu ammonis (the CA1 to CA3 regions) (Figure 1). The principal neurons of the hippocampal formation consist of the pyramidal and the granule neurons; all of which are known to be glutamatergic excitatory neurons and participate in a unidirectional tri-synaptic neuronal circuit [1]. The tri-synaptic circuit begins with the pyramidal neurons located in the EC, projecting to the granule neurons in the DG via the performant pathway. The DG granule neurons send their axons to the CA3 pyramidal neurons through the mossy fiber, which in turn extends to the CA1 pyramidal neurons via the Schaffer collateral. The CA1 neurons project back to the deep layers of the EC, closing circuit [2]. Besides having extensive connections to the DG, the EC also directly projects to the CA1 region via the temporal-ammonic pathway. Thus, the CA1 neurons can compare and integrate signals from the EC and the CA3 [3].

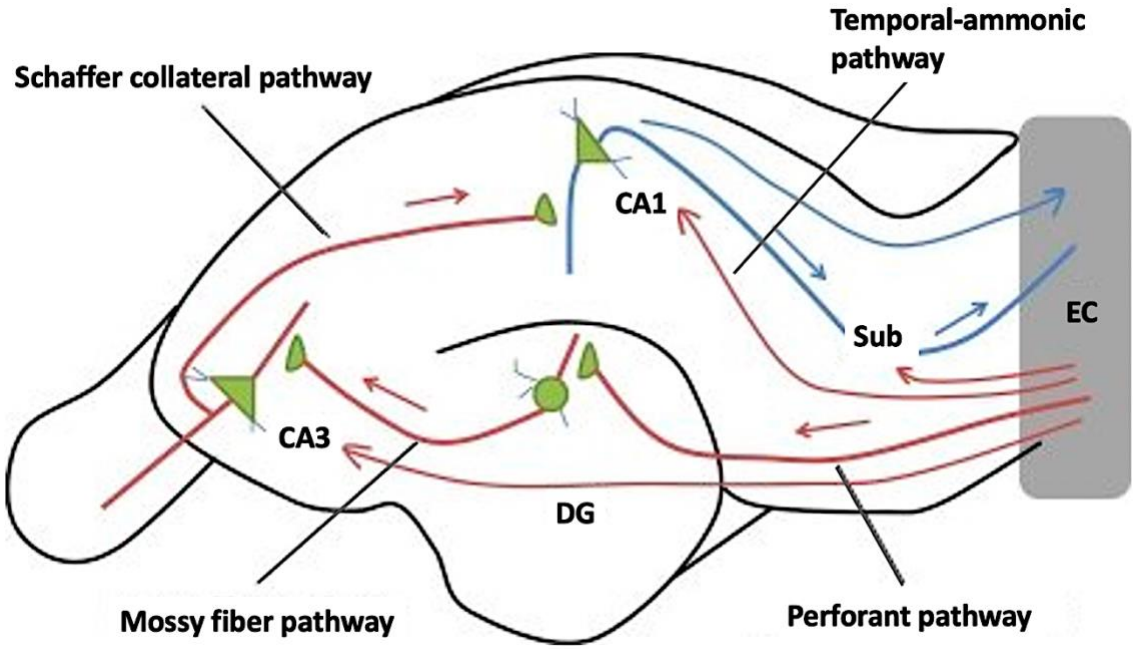

Figure 1: The input and output pathways of hippocampal formation. Entorhinal cortex (EC) is the main input to the hippocampus. The EC projects to the dentate gyrus (DG) via the performant pathway and provides critical input to the CA3 region via the mossy fiber pathway, then to the CA1 by means of the Schaffer collateral pathway. The major output neurons of the hippocampus are the CA1 pyramidal neurons, the subiculum (Sub), and deep layers of the EC; modified from Zang and Zhu (2011) [4].

1.1.2 The hippocampal function and neurons

The hippocampal formation plays a pivotal role in multiple cognitive functions, including episodic memory [5,6,7], spatial navigation [8], and emotion-related processing [9]. The principal neurons in the hippocampal tri-synaptic circuitry fire temporally- and spatially-modulated spikes whenever the animal is exposed to a new environment and form a neural representation of space within the brain [8]. These consist of pyramidal and granule cells, all of which are believed to be glutamatergic excitatory neurons. Pyramidal neurons in the CA3 region have larger cell bodies (~25um diameter) than those in the CA1(~15um). All hippocampal pyramidal cells are aligned in the same orientation, with the apical dendritic trees expanding toward the center of the C-shaped semicircular stratum oriens. The principal

neurons in the DG are the granule neurons, which have relatively small cell bodies (~10um diameter) and share the same orientation with each other. Although there are several types of inhibitory interneuron cell bodies scattered throughout the whole hippocampal formation, most of these interneurons are presumed to be gamma-aminobutyric acid (GABA)ergic [1]. There are notably fewer number of interneurons than the principal neurons; ten to fifteen percent of all hippocampal neurons. This pattern of connectivity (lower numerical density of interneurons) allows them to have substantial influence on overall hippocampal function [10]

1.2 Transcriptional regulations in the hippocampal memory formation

1.2.1 DNA methylation in the hippocampal memory formation

DNA methylation is predominantly found at the 5' position of the DNA base cytosine, adjacent to guanine nucleotides, within CpG rich region [11]. The catalytic activity of the methylation process is governed by a family of developmentally regulated enzymes called DNA methyltransferases (DNMTs). The methylation of promoter sequences activates transcriptional silencing, and methylation within gene bodies is considered to suppress cryptic start sites within active genes [12,13]. DNA methylation represses gene expression by increasing compaction of nucleosomes [12], by decreasing the affinity of transcription factors (TFs) that recognize unmethylated cytosine [14], or by recruiting other chromatin remodelers that recognize 5'-methylcytosine [15]. The methylation of CpG rich sites plays a critical role in the regulation of gene expression in the CNS since the brain-specific promoter-related sequences are highly enriched in CpG sites [16]. In the context of memory processing, DNA methylation is regulated in an experience-dependent manner by neural activity. Upon the exposure to contextual fear conditioning, DNMT expression is rapidly increased within the hippocampus, leading to downregulation of memory suppressor gene, calcineurin [17].

Conversely, the induction of hippocampal synaptic plasticity is inhibited when treated with DNMT blocker [18]. These reports suggest that DNA methylation plays a role in repression of genes that act to hinder memory formation.

1.2.2 Post-translational histone modification in the hippocampal memory formation

Post-translational histone modifications, particularly histone acetylation and methylation, have been extensively studied in the context of hippocampal learning and memory [19]. Histone acetylation involves the addition of an acetyl group to a lysine residue at the N-terminal of histone tails and is mainly associated with active gene expression. It is regulated by opposing actions of histone acetyltransferases (HATS) and deacetylates (HDACs). Histone H3 acetylation levels are increased in the hippocampus, following contextual fear conditioning [20] and are mediated by NMDA receptor stimulation and by activation of extracellular signal-regulated kinase (ERK) signaling, which leads to an influx of calcium ions into neurons and initiates memory acquisition in the hippocampus [21].

Unlike histone acetylation, histone methylation occurs on both lysine and arginine residues. It can activate or repress gene expression depending on the position of amino acid residue and the number of methyl groups (mono-, di-, and tri-) added, which confers further complexity in chromatin remodeling. For instance, mono-, di-, and tri-methylation of histone H3 lysine 4 (H3K4me1/2/3) is associated with active chromatin regions [22], while tri-methylation of histone H3 lysine 27 (H3K27me3) and histone H3 lysine 9 (H3K9me3) are linked to repressed chromatin [23]. Among other epigenetic modifications, histone H3 methylation is recognized as a plausible mechanism for memory storage due to its capability to mediate long-lasting changes in gene expression driven by experience. For example,

H3K4me3 and H3K9me2 were both increased in bulk chromatin extracts from the CA1 pyramidal neurons in rats 1 hour after contextual fear conditioning and then returned to baseline levels twenty-four hours later. Correspondingly, the fear-induced increases in H3K4me3 were linked to the promoters of the early-memory-associated genes, such as *Zif268* and *Bdnf* [24]. Taken together, these studies demonstrated that transcriptional activation and repression through histone H3 methylation are both involved in hippocampal memory processing.

The establishment, maintenance, and removal of methyl-groups is mediated by various chromatin remodeling complexes. For example, the methylation of H3K4 is primarily catalyzed by the Trithorax group (TrxG) complexes [25]. In mammals, all TrxG complexes contain the core proteins (ASH2L, RBBP5, and WDR5, and DPY30), and one of the six histone methyltransferases; KMT2A (MLL1), KMT2B (MLL2), KMT2C (MLL3), KMT2D (MLL4), SET1A, and SET1B [26]. While the TrxG core proteins regulate complex activity and stability, additional TrxG complex-specific co-factor proteins facilitate complex function and contribute to site-specific recruitment through unique interactions with TFs [27,28]. For instance, H3K4me3 is catalyzed by KMT2A/2B and SET1A/1B complexes when in association with the subunits menin and WDR82, respectively. Recent advances in next-generation sequencing have revealed that all six KMTs are strongly expressed in the hippocampus throughout the life span of humans [29], indicating potential contributions to hippocampal neurogenesis and memory processing. Indeed, deletion of *Kmt2a* and that of *Kmt2b* in the hippocampal neurons cause a significant reduction of H3K4me3 around transcriptional start sites (TSS) of genes involved in synaptic plasticity, leading to spatial memory deficits in mice [30,31]. Nonetheless, the interesting question remains whether the resulting memory deficits are due to the loss of

H3K4me or due to the loss of KMT2A/KMT2B itself. Importantly, TrxG complexes have non-catalytic co-activator functions in addition to the methyltransferase activities. Further, the enzyme-independent role appeared to have a greater transcriptional regulatory role than their catalytic activity [32,33]. For instance, loss of KMT2C and KMT2D proteins considerably reduce occupancy and transcription of RNA polymerase II (Pol II), while disruption of the KMT2C/KMT2D catalytic domain in the embryonic stem cells (ESC) does not affect self-renewal and has a minor effect on transcription [32,34,35]. The non-enzymatic co-activator roles of TrxG complexes can be achieved by direct or indirect interactions with other chromatin regulators. In agreement, KMT2A/2B complexes interact with the Pol II-associated factor PAF1 and the SET1A/1B complex component WDR82 interacts with Pol II [28] Moreover, several reports indicated that H3K4me is not vital for activation or maintenance of gene expression. For instance, catalytically deficient MLL3/4 mutant mouse ESC lines results in the loss of H3K4me1, which has a minor effect on transcription [34]. Similarly, disruption of H3K4 methyltransferase activity either via mutation of the *Mll3* and *Mll4 Drosophila* homolog *Trr* or via loss of the MLL3/4 catalytic SET domain in mouse ESCs results in minimal changes in gene expression [35]. Hödl and Basler (2012) also found that transcriptional activation and maintenance are unaffected in the absence of H3K4me by generating non-methylatable H3K4 *Drosophila* mutants [36]. Further, recent evidence indicated that activation of developmentally regulated genes in *Drosophila* and in *C. elegans* can occur in the absence of H3K4me [71]. In agreement, our previous data showed that H3K4me is not required for bulk gene expression but is necessary for transcriptional stability [32]. Given these conflicting reports, the role of H3K4me in mediating neuronal gene expressions remains unclear.

Although H3K4 methylation is associated with active chromatin, its precise function in gene activation is not fully understood. Some reports suggest it is involved in the establishment and/or maintenance of active chromatin. For instance, gene activation by KMT2B *in vitro* was dependent on the catalytic H3K4 methyltransferase activity [72]. In mouse ESCs, catalytically deficient KMT2B hindered the activation of genes necessary for primordial germ cell specification [73]. Rather than initiation of transcription, H3K4 methylation is linked to the maintenance of lineage-specific gene expression in several cell types [74,75]. Benayoun, B. A. *et al.* (2014) also reported that H3K4me3 domains that spread more broadly over genes in a given cell type selectedly mark genes important for the identity and function of that cell type [77]. Further, H3K4 methylation facilitates enhancer-promoter interactions. In differentiating mouse ESCs, MLL3/4-dependent deposition of H3K4me1 at enhancers was interconnected with increased levels of chromatin interactions while loss of H3K4me1 resulted in gene activation defects during differentiation [76]. Also, H3K4me3 may contribute to stable gene expression by recruiting the general transcription factor IID and allowing efficient Pol II loading during initiation of transcription [27,28].

Within the TrxG complexes, the core subunit protein DPY30 is essential for full methyltransferase activity but is not required for the formation of the TrxG complexes [70]. In the absence of DPY30, the TrxG complex H3K4 methyltransferase activity is marginally decreased *in vitro* but completely lost *in vivo*, indicating the potential contribution of DPY30 as a catalytic enhancer [45]. The role of DPY30 in hippocampal plasticity has not been elucidated, but DPY30 has reported roles in a proliferation and differentiation of postnatal neural stem cells (NSCs) [56]. Deletion of *Dpy30* in NSCs from embryonic day 13.5 (E13.5) resulted in disruption of neural development, including deformed DG and enlarged lateral

ventricles in mice. As a consequence of developmental abnormalities, the *Dpy30* knockout (KO) mice exhibited growth retardation and ataxia and died between postnatal day 20 (P20) and P27. Importantly, a significant reduction of H3K4me3 was observed from cells within DG and subventricular zone (SVZ) where postnatal neurogenesis takes place. Transcriptome analysis also revealed downregulation of neuronal markers in the DG and gliogenic markers in the SVZ of KO mice, suggesting perturbed neurogenesis and gliogenesis in DG and SVZ, respectively. Further, H3K4me3 was reduced at several neuronal and gliogenic genes upon loss of DPY30 *in vitro*. Although these results support a cell-intrinsic role of DPY30 and its associated H3K4me in the fate determination of NSCs, it remains unknown if H3K4me is implicated in regulating activities of mature neurons. Particularly due to early postnatal lethality of the mouse model, the effect of H3K4me depletion on memory formation has not been demonstrated.

1.3 H3K4 methylation in Alzheimer's disease and other neurological diseases

1.3.1 What is Alzheimer's disease?

Alzheimer's disease (AD) is an age-related neurodegenerative disorder, affecting 50 million people world-wide. The common symptoms of AD include extensive memory loss, mood swing, confusion, and difficulty with language. In most cases, AD progresses to dementia and ultimately leads to death [37]. The pathology of AD is characterized by the accumulation of abnormal aggregates composed of amyloid beta (Ab) and tau between nerve cells, which eventually form amyloid plagues and neurofibrillary tangles in the brain. The combined insults of Ab and tau accumulation are thought to promote progressive synaptic failure and neuronal loss, and brain atrophy. The hippocampus, especially the CA1 region, is

considered particularly vulnerable as it constitutes the primary output of the hippocampus and one of the first regions affected in AD [38,39].

1.3.2 Histone H3 lysine 4 methylation in Alzheimer's disease and other neurological diseases

Human clinical data have supported the idea that H3K4 methylation is important for cognitive processing. Support for this comes from the observation that mutations in members of the complexes that mediate H3K4 methylation cause a series of rare neurodevelopmental and neuropsychological disorders. For instance, *de novo* mutation in *Kmt2a* is associated with Wiedemann-Steiner syndrome [40]. Heterozygous variants in *Kmt2e* have been linked to autism spectrum disorder [41]. Loss of function mutations in *Kdm5a* is found in patients with intellectual disability [42]. Very few studies have so far investigated a potential role for H3K4 methylation in the pathology of AD. In a mouse model of AD, CK-p25 mice, H3K4me3 is increased at proinflammatory genes and decreased at genes involved in learning and memory [43]. Recently, it was shown that *Kmt2a* is downregulated in the hippocampus of CK-p25 mice. In line with this downregulation, the same study found that hippocampus-specific deletion of KMT2A produced a significantly similar alteration in gene expression in the hippocampus, as did the CK-p25 mouse model of AD [31]. With respect to clinical data, a decrease in nuclear H3K4me3 concomitant with increased abnormal cytoplasmic H3K4me3 was observed [44].

1.4 Study hypotheses and aims

I hypothesize that the catalytic activity of Trithorax group complexes, and thus H3K4 methylation is required for proper formation of hippocampal memory. Furthermore, I hypothesize that the level of H3K4 methylation is reduced in the hippocampal neurons in

Alzheimer's disease. To test these hypotheses, I employed the following aims; 1) establish mouse model with hippocampal specific loss of H3K4 methylation and investigate if the mice exhibit any behavioural abnormalities related to hippocampus, 2) examine if H3K4 methylation is altered in the hippocampus of Alzheimer's disease donors.

Chapter 2: Materials and Methods

2.1 Generation of mouse model and genotyping

All mice were housed at the British Columbia Children's Hospital Research Institute (BCCHRI) Animal Care Facility (ACF) and ethical procedures were followed according to the protocols approved by the University of British Columbia Animal Care Committee. All mice were maintained on a regular chow diet ad libitum and housed up to 5 mice per cage on a 12-hour light/dark cycle.

In this study, I examined the catalytic activity of TrxG complexes by targeting *Dpy30*. DPY30 is one of the TrxG core subunit proteins and is essential for the catalytic activity *in vivo* [45] but is not required for TrxG complex formation or recruitment of Pol II [46]. Two heterozygous *Dpy30*$^{tm1a(KOMP)Wtsi}$ male mice on a C57BL/6NJ background were obtained from the International Knockout Mouse Consortium (EMMA ID EM:09575) and bred to *Rosa26*^{FLPe} female mice (The Jackson Laboratory, Stock No. 009086). This removed the Dpy30 knockout-first cassette, containing a splice acceptor between FRT sites) and generated heterozygous floxed *Dpy30* mice. Progeny were bred to produce floxed *Dpy30* mice when crossed Cre driver mice, conditional deletion of *Dpy30* exon 4 in the post-mitotic excitatory neurons of the hippocampus was attained. Exon4 is the largest coding exon, and its deletion causes a frameshift mutation in every protein-coding transcript and generates a non-functional protein. The Cre driver strain B6.Cg-Tg(Camk2a-cre)T29-1Stl/J was obtained from the Jackson Laboratory (Stock No. 005359). *Camk2a*-Cre; *Dpy30*$^{flox/flox}$ knockout mice (*Dpy30⊿H*) were generated by breeding either male or female *Camk2a*-Cre; *Dpy30*$^{flox/wt}$ transgenic mice to *Dpy30*$^{flox/flox}$ animals. For all the experiments conducted in this study, I used male and female 3 to 5 months old *Dpy30⊿H* and *Dpy30*WT control (*Camk2a*-Cre; *Dpy30*$^{wt/wt}$) mice. For

histological analyses, *Dpy30⊿H* mice were crossed to reporter mice with *Rosa26-lox-STOP-lox-tdTomato,* which were gifted from Dr. Francis Lynn (University of British Columbia). The reporter (tdTomato^{+}) mice allowed us to aid in visualizing recombination by fluorescently label nuclei of cells that have had Cre activity [47]. All knockout mice were compared to littermate controls (*Dpy30$^{flox/flox}$* and *Dpy30$^{flox/wt}$*). Genotyping primers are listed in Table 1.

Table1: Genotyping primer sequences

Genotyping PCR	Left Primer Sequence	Right Primer Sequence
Mutant *Dpy30^{tm1a}*	AATTCAGCACCAGCACTTGG	TCGTGGTATCGTTATGCGCC
Floxed *Dpy30*	GTGAGTGCCAGGAACCAAAT	GTTGTGAGCTGCCATGAAGA
Camk2a-Cre Transgene	GCGGTCTGGCAGTAAAAACTATC	GTGAAACAGCATTGCTGT CACTT
Camk2a-Cre Internal Control	CTAGGCCACAGAATTGAAAGATCT	GTAGGTGGAAATTCTAGCATCATCC
Tomato Mutant	TAGAGCTTGCGGAACCCTTC	AGGGAGCTGCAGTGGAGTAG
Tomato Common	CTTTAAGCCTGCCCAGAAGA	

2.2 Microscopy

2.2.1 Tissue preparation and sectioning

Animals were perfused transcardially with phosphate-buffered saline (PBS) followed by 4% paraformaldehyde (PFA) pH7.2. The brains were removed and postfixed in 4% PFA for 24 hours at 4ºC and then stored in PBS until ready for sectioning. The whole brain of each animal was cut into 45 μm coronal sections using a vibrating microtome (Leica) and the tissue sections were stored at 4ºC in PBS.

2.2.2 Fluorescent immunohistochemistry, imaging, and analysis

Free-floating immunohistochemistry was used for rodent brain histological analysis. The coronal sections were washed in PBS for 3x10 minutes, followed by blocking (10% Goat serum in PBS-T (PBS with 0.1% Triton-X100)) for 2 hours at room temperature. Primary antibodies were incubated at 4^{o}C overnight with dilutions in 50% blocking solution and 50% PBS-T (see Table 2 for antibody information). The following day, sections were washed 3x10 minutes in PBS and incubated with secondary antibodies in PBS for 1 hour at room temperature. Subsequently, the sections were washed in PBS for 10 minutes and carefully put on the glass slide with a paintbrush. After 15 minutes of drying period, the slides were rehydrated in PBS and mounted with Prolong Gold mounting solution. I used Leica TCS SP8 Confocal microscope for imaging and CellProfiler v2 software with custom pipelines for analysis.

Table 2: List of primary and secondary antibodies used in fluorescent immunohistochemistry.

Antibody	Host Species	Manufacturer	Catalog No.	Dilution
Dapi		Thermo Fisher Scientific	D9542	1:5000
Doublecortin (Dcx)	Rabbit	Cell Signaling	#4604	1:500
DPY30	Rabbit	Abcam	Ab214010	1:1500
H3K4me3	Rabbit	Cell Signaling	C42D8	1:1500
NeuN	Mouse	MilliporeSigma	MAB377	1:750
Alexa Fluor 488 anti-Rabbit	Donkey	Thermo Fisher Scientific	A-21206	1:500
Alexa Fluor 546 anti-Mouse	Goat	Thermo Fisher Scientific	A-11003	1:500

2.3 Behavioural studies

2.3.1 Sample selection and preparation

Based on the histological analysis (significant loss of H3K4me3 at 3 months of age), 3-months-old and older *Dpy30*ΔH and *Dpy30*WT mice were subject to the behavioural studies. I completed a comprehensive behavioural test battery in order of increasing invasiveness (open field test, novel object recognition test, and Morris water maze test) and conducted twice. For the first cohort, the animals were originally at 3 to 4 months of age but turned to 5-months old by the end of experiments. The second cohort consisted of 10-months old litter mates, which were only exposed to open field and novel object recognition tests. The summaries of behavioural studies are seen in Table 3 and Table 4.

Table3: The number of male (M) and female (F), knockout (*Dpy30*ΔH) and wild-type (*Dpy30*WT) mice included in statistical analyses.

Cohort	#1 (3 to 5 months of age)				#2 (10 months old)			
Genotype	*Dpy30*ΔH		*Dpy30*WT		*Dpy30*ΔH		*Dpy30*WT	
Sex	M	F	M	F	M	F	M	F
Number	6	4	8	3	2	3	2	3

Table 4: The order and general procedure of tests within the test battery completed by *Dpy30*ΔH and *Dpy30*WT mice.

Test Order	Behavioural Test	No. of days of testing	Training procedure	No. of days before subsequent test is initiated.
1	Open field test	1	5 minutes trial	1-3
2	Novel object recognition test*	1	5 minutes of habituation followed by 10 minutes of familiarization. (90 minutes later) 10 minutes of novelty measurement	1-3
3	Morris water maze test	15	7 days of acquisition training (4 trials/day) Acquisition probe (1 trial) 5 days of reversal training (4 trials/day) Reversal probe (1 trial) 1 day of visible platform training (4 trials)	1-3

Note* All the experiments were conducted between 12PM to 5:30PM in order to keep consistency of measurement. I measured the maximum of 5 mice per day for the novel object recognition test.

2.3.2 Open field (OF) test

The open field (OF) (40cmx40cm) was constructed from a clear Plexiglas and consisted of an open square box. The three of four walls (36cm high) of the maze were stuck to black cardboard. However, one of the walls was left transparent to allow mice to be visible when in the apparatus. The CCD camera was positioned right above the apparatus and Webcam was placed in front of a transparent wall of the maze. The animals were placed into one of the corners of the OF and allowed to explore a single 5 minutes of trial. Time spent in an imaginary center square of the open field (10cmx10cm) and velocity of walking was recorded using the video-based EthoVision tracking system (Noldus, Wageningen, The Netherlands).

2.3.3 Novel object recognition test (NORt)

Experimental settings of the novel object recognition tests (NORt), including apparatus and camera positions, were unchanged from the OF test (in Chapter 2.3.2). Mice were habituated to an empty arena for 5 minutes and returned to a cage. After brief cleaning of arena with 70% ethanol, the animals were presented with two identical ("familiar") objects for 10 minutes. Ninety minutes after the familiarization training, the mice were re-exposed to the arena with two objects, one "familiar" and the other "novel" (unfamiliar) object for 10 minutes. The "familiar" and "novel" objects were constructed from plastic Lego bricks and 50 ml falcon tubes containing colored pencils. The time spent exploring each object was recorded and analyzed retrospectively using Webcam recordings.

2.3.4 Morris water maze (MWM) test

The Morris water maze (MWM) test consisted of a circular pool (110cm diameter) with 25cm high walls. The pool was filled with 23ºC water to a depth of 15cm, which was made opaque with non-toxic liquid tempera paint. A circular escape platform (9cm diameter, 14cm height) was placed in the pool, 1cm beneath the surface of the wall. Small grooves were etched on the top of the escape platform, and a small rubber tube was placed around the escape platform (1cm below top), in order to assist mice in climbing onto the escape platform. Extra-maze cues (triangular and square shaped black cardboard) were stuck to the walls of behavioural test room and were visible from the water surface. Mice completed four phases of testing; acquisition training (4 trials/day for 7 days), acquisition probe (single trial for a day), reversal training (4 trials/day for 5 days), reversal probe (single trial for a day), and visible platform training (single trial for a day). Figure 2 depicted experimental design of the MWM.

The hidden platform was located at zone 1 during acquisition training and was relocated to the zone 3 for the reversal training. For each trial, the animal was released into the pool from one of the four positions/directions (N, S, E, W) around the edge of the pool and was given a maximum of 60 seconds to find the platform, after which it was guided to the platform and remained on the platform for roughly 10 seconds before being returned to the holding cage. The EthoVision tracking system recorded the movement of mice in the MWM, using a CCD camera positioned above the maze.

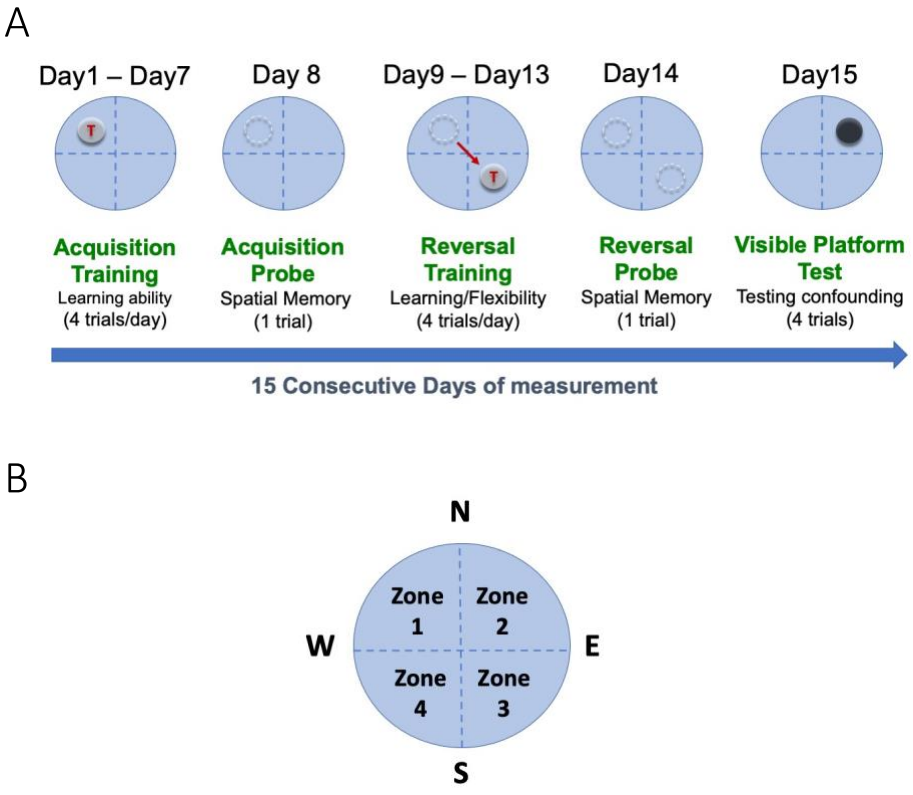

Figure 2: Experimental design of the Morris water maze. (A) Morris water maze consists of seven days of acquisition training (4 trials/day), one day of acquisition probe test (single trial), five days of reversal training (4 trials/day), one day of reversal probe (single trial), and one day of visible training (4 trials). **(B)** For each trial, the animal was released into the pool from one of the four positions/directions (N, S, E, W) around the edge of the pool. The hidden platform was located at zone 1 during acquisition training and moved to zone 3 for reversal training.

2.4 Alzheimer's disease study

2.4.1 Preliminary histology study on rodent Alzheimer's disease model

Rodent Alzheimer's disease (AD) model, 5XFAD (Tg6799), was obtained from the Jackson laboratory and was used for the preliminary histology study. This model contains five human familial AD gene mutations – Amyloid Precursor Protein (APP) mutations from the Swedish, Florida and London families, along with two mutations in presenilin-1 [48]. Free-floating immunohistochemistry was performed as noted at section 2.2.2 to examine the intensity of H3K4me in the hippocampus of 5XFAD and control mice at 9 months of age.

2.4.2 Sample selection for post-mortem human brain samples

Age- and sex-matched frozen brain samples from healthy and AD donors (diagnosis confirmed by neuropathological reports; CERAD criterion) were obtained from the Douglas-Bell Canada Brain Bank (Douglas Mental Health University Institute, Montreal, Canada). Utilization of these samples was approved by both the Douglas Institute's research ethics board and the Children's and Women's Research Ethics Board. A brief summary of subject data provided by the brain bank is seen in Table 5. The frozen samples were stored at -80^{o}C.

Table 5: Subject data for Alzheimer's disease (AD) patients and healthy (Control); male (M) and female (F) provided by Douglas-Bell Canada Brain Bank.

Group	ID	Sex	Age
AD	DH1787	M	87
	DH1821	M	74
	DH1822	M	88
	DH1880	M	86
	DH1780	M	90
	DH1806	F	86
	DH1748	F	74
	DH1792	F	89
	DH2060	F	77
	DH2090	F	89
Control	DH1582	M	85
	DH1763	M	83
	DH1881	M	89
	DH1990	M	72
	DH2010	M	76
	DH1783	F	91
	DH1194	F	92
	DH1888	F	72
	DH1900	F	67
	DH1291	F	85

2.4.3 Western blotting on human sample

The frozen brain samples for immunoblotting were taken from -80^{o}C freezer and thaw on ice. Protein extracts were prepared from the tissue samples by sonication in RIPA Buffer (Pierce) on ice. The tissue homogenates were centrifuged at 13200rpm at 4^{o}C for 20 minutes and the supernatant was transferred to a clean tube and stored at -80^{o}C.

Pierce BCA Protein Assay Kit (ThermoFisher; 23225) was used to quantify the protein concentration from cell lysates made by and samples were denatured in 1x SDS loading dye (0.1% 2-Mercaptoethanol, 0.0005% Bromophenol blue, 10% Glycerol, 2% SDS, and 63 mM Tris-HCl pH 6.8) by boiling for 10 minutes. SDS-PAGE (10-15%)

1.5mm 10-well gels were cast using the Mini-PROTEAN casting system (Bio-Rad; 1658006FC) as required based on protein size. Gels were placed in a Mini-PROTEAN tetra cell (Bio-Rad; 1658004EDU) and topped up with 1x running buffer (192mM Glycine, 25mM Tris base, 1% SDS, in ddH_2O). The protein (10μg) was loaded and run alongside Precision Plus Protein ladder (Bio-Rad; #1610375).

Polyvinylidene difluoride (PVDF) membranes were soaked in 100% methanol for a minute and placed in 1x transfer buffer (192mM Glycine, 25mM Tris base, 20% Methanol, in ddH_2O). Gels were placed in 1x transfer buffer and assembled with PVDF membranes using a Criterion Blotter (Bio-Rad; 1704070). Transfer was performed at room temperature 150V for an hour. Following transfer, the membrane was rinsed in 1xTBST (20mM Tris pH7.6, 150mM NaCl, 0.1% (v/v) Tween-20 in ddH_2O), blocked for an hour in 5% (w/v) skim milk powder in TBST) at room temperature, and probed with primary antibodies overnight in 5% (w/v) BSA in TBST at 4^oC. The next day, after washing membrane three times with TBST, HRP-linked secondary antibodies were added and were incubated for an hour at room temperature. After brief washing in TBST, the membrane was developed using Luminata Crescendo Western HRP substrate (EMD Milipore; WBLUR0500) and exposed using Bioflex MSI Film (Mandel Scientific; MED-CLMS810). For normalizing to total H3, membranes were stripped for 20 minutes in mild stripping buffer (200mM glycine, 0.1% (w/v) SDS, 1% (v/v) Tween-20, pH2.2) at room temperature, rinsed twice in PBS and twice in TBST for 10 minutes each, then re-blocked and probed for histone H3. Antibodies used for immunoblotting are seen in Table 6. Band intensities were quantified using ImageJ.

Table 6: List of primary and secondary antibodies used in immunoblotting.

Antibody	Host Species	Manufacturer	Catalog No.	Dilution
H3	Rabbit	Abcam	Ab1791	1:1000000
H3K4me1	Rabbit	Abcam	Ab8895	1:50000
H3K4me3	Rabbit	Cell Signaling	C42D8	1:1100
IgG-HRP secondary antibody	Rabbit	Santa Cruz	Sc-2768	1:10000

2.5 Statistical analysis

Statistical analyses were performed using GraphPad Prism 8 Software (GraphPad Software, La Jolla, CA, USA). Data are expressed as mean ± standard error of the mean (SEM) unless otherwise specified and all experiments were carried out at a minimum in triplicate. Statistical significance was determined using unpaired, two-tailed Student's t-tests with Welch's correction for comparisons between two groups. Data from the MWM was analyzed by two-way repeated-measures (RM) ANOVA with genotype as the between-subjects factor and days as the within-subjects factor followed by Bonferroni post-hoc test. One-way ANOVA with Dunnett's post hoc test was used for comparisons between genotypes and within days. Results were considered significant when $P < 0.05$, with *indicating $P < 0.05$, ** indicating $P < 0.01$, *** indicating $P < 0.001$, and **** indicating $P < 0.0001$.

Chapter 3: Results

Post-mitotic excitatory neuronal specific deletion of *Dpy30* in the hippocampus led to the loss of H3K4me3 in *Dpy30*ΔH mice by three months of age (Figure 3-5). The animals exhibited hippocampus-associated behavioural abnormalities, including a presence of anxiety-like behaviour (Figure 6), impaired recognition memory (Figure 8), and a significant deficit in reversal memory (Figure 9). The level of H3K4me3 was decreased in the CA1 pyramidal neurons of 5XFAD mice. Similarly, significant reduction of H3K4me3 was observed from the hippocampus of Alzheimer's disease donors, compared with the samples from healthy controls (Figure 12).

3.1 Cre recombinase activities of the model

First, I focused on the general characterization of mouse model. According to the original publication describing the *Camk2a*-Cre strain, the Cre recombination is initiated by postnatal day 19 (P19) and the level of Cre mRNA in the hippocampus becomes substantial by P23 [49]. Hence, I examined the time course of Cre/loxp recombination and quantified the fraction of DPY30 positive and H3K4me3 positive cells in the hippocampus of *Dpy30*ΔH model from one to three months of age. By 1 month of age, *tdTomato* expressing cells were observed from the CA1 region of hippocampus in the *Dpy30*ΔH mice, but *Dpy30* was fully expressed in the region (Figure 3A). *Dpy30* expression was significantly deleted in the mice by 2 months of age (Figure 3C; $P < 10^{-6}$) and became nearly unidentified by 3 months of age (Figure 3B). Importantly, there were a few DPY30-positive neurons observed at 3 months, but these cells did not express *tdTomato* (and thus Cre negative cells), which further confirms the specificity of Cre-loxP recombination in this model (Figure 3A). Significant loss of H3K4me3 was

observed from 3 months of age (Figure 4C; $P < 10^{-6}$) – a month delayed from significant deletion of DPY30 due to slow turnover rate of histone protein. As seen in the expression of *Dpy30*, H3K4me3 was observed from *tdTomato*-negative cells (Figure 4A). In agreement with the original article [49], *Camk2a*-Cre activity was restricted to post-mitotic neurons as co-expression of *tdTomato* and immature neuron marker, doublecortin (Dcx), was not identified (Figure 5A). Hippocampal morphology appeared to be unaffected throughout the first three months of postnatal period in *Dpy30*ΔH mice. A densely packed C-shaped band of granule cells was observed from both *Dpy30*ΔH and *Dpy30*WT mice (Figure 5B). I also did not detect any abnormalities of hippocampal neurogenesis. There was a number of Dcx-expressing cells in the hippocampus of three-months old *Dpy30*ΔH mice even after a significant loss of H3K4me3 (Figure 5A).

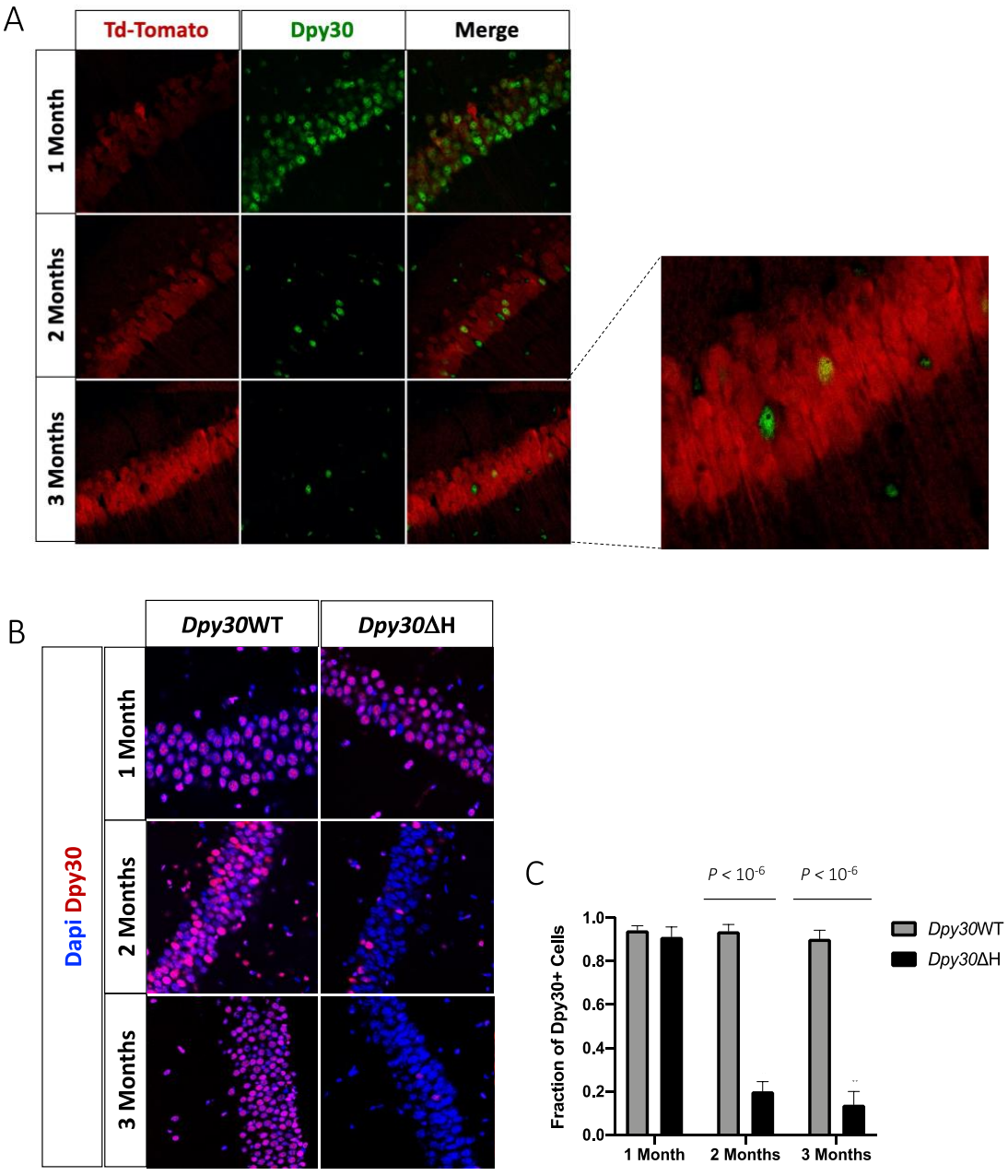

Figure 3: Significant deletion of *Dpy30* expression was observed in *Dpy30*ΔH mice by 2 months of age. (A) Immunofluorescent staining of *tdTomato* (red) and *Dpy30* (green) in the CA1 hippocampal region of 1 to 3 months old *Dpy30*ΔH mice. **(B)** Immunofluorescent staining of *Dpy30* (red) and Dapi (blue) in the CA1 region of the hippocampus in 1 to 3 months old *Dpy30*WT and *Dpy30*ΔH mice. **(C)** Quantification of the number of DPY30-positive cells in the CA1 hippocampal region of *Dpy30*WT and *Dpy30*ΔH mice normalized against Dapi nuclear dye; n=3/group Data are presented as mean± SD; unpaired, two-tailed Student's t test with Welch's and Benjamini-Hochberg 1% FDR correction for multiple comparisons. Only $P < 0.05$ is shown.

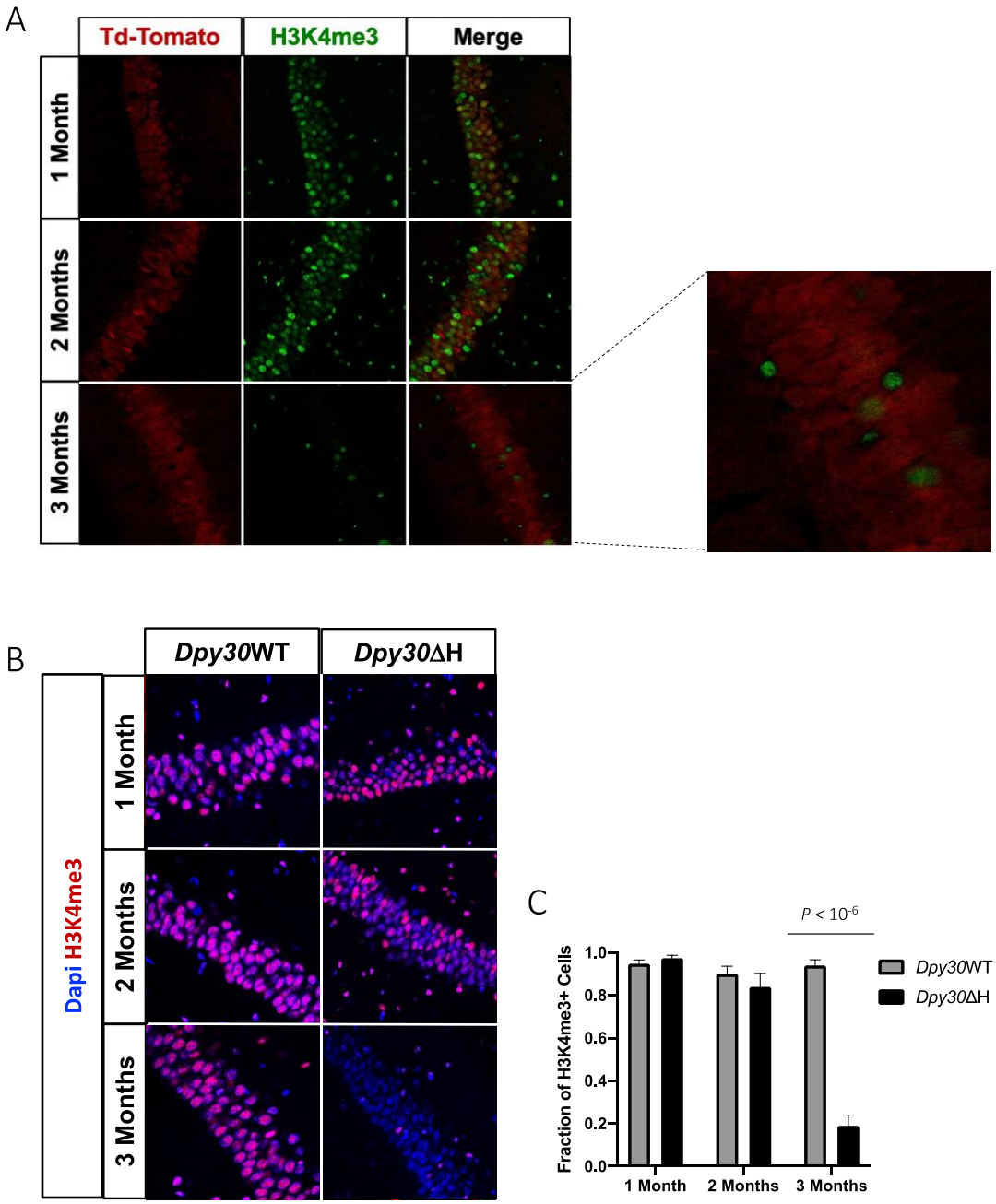

Figure 4: Significant loss of H3K4me3 was observed in *Dpy30*ΔH mice by 3 months of age. (A) Immunofluorescent staining of *tdTomato* (red) and H3K4me3 (green) in the CA1 hippocampal region of 1 to 3 months old *Dpy30*ΔH mice. **(B)** Immunofluorescent staining of H3K4me3 (red) and Dapi (blue) in the CA1 region of the hippocampus in 1 to 3 months old *Dpy30*WT and *Dpy30*ΔH mice. **(C)** Quantification of the number of H3K4me3 positive cells in the CA1 hippocampal region of *Dpy30*WT and *Dpy30*ΔH mice normalized against Dapi nuclear dye; n=3/group. Data are presented as mean± SD; unpaired, two-tailed Student's t test with Welch's and Benjamini-Hochberg 1% FDR correction for multiple comparison. Only $P < 0.05$ is shown.

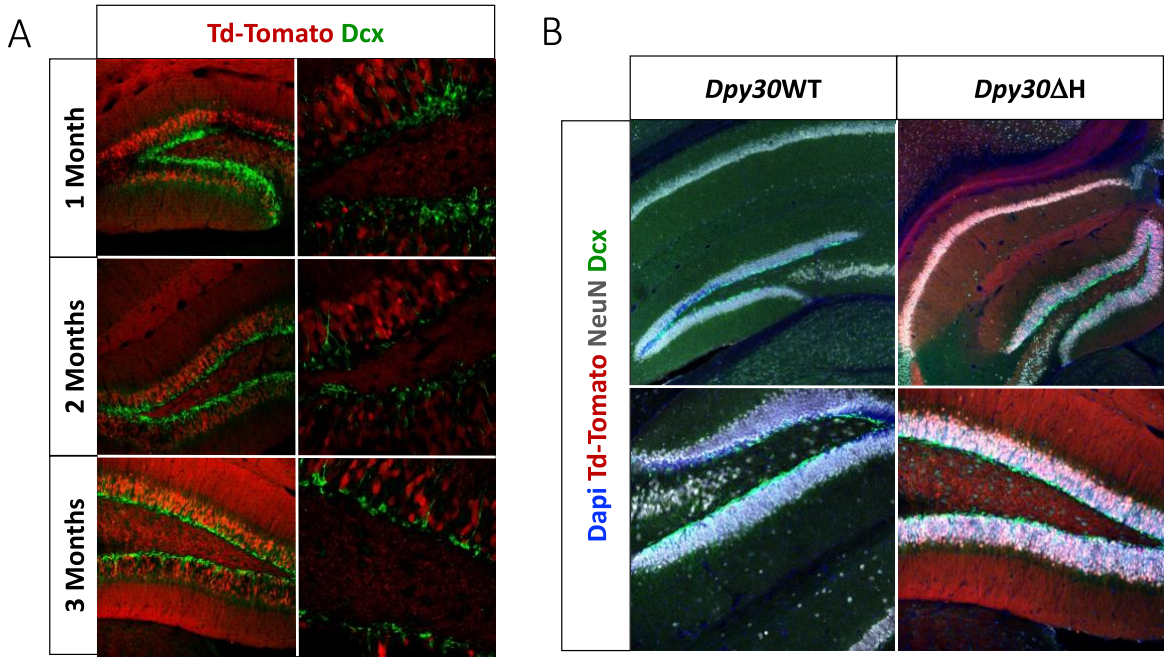

Figure 5: Post-mitotic neuron-specific Cre activity did not affect hippocampal gross anatomy and neurogenesis in *Dpy30*ΔH mice. (A) Immunofluorescent staining of *td-Tomato* (red) and immature neuron marker, doublecortin (*Dcx*/green), in the dentate gyrus of 1 to 3 months old *Dpy30*ΔH mice. **(B)** Immunofluorescent staining of Dapi (blue), td-Tomato (red), mature neuron marker, *NeuN* (gray), and *Dcx* (green) in the hippocampus (top) and dentate gyrus (bottom) of 3 months old *Dpy30*WT and *Dpy30*ΔH mice.

3.2 H3K4 methylation is required for proper formation of hippocampal memory

I completed a comprehensive behavioural test battery on *Dpy30*ΔH and *Dpy30*WT mice at 3-month of age and older to examine whether the loss of H3K4me affects the hippocampus-responsible behaviours. In the order of increasing invasiveness, I first performed an open field test (3.3.1) to measure the horizontal activity and the presence of anxiety-like behaviour, then assessed the novel object recognition test (3.3.2) to examine the recognition memory (the ability to recognize previously encountered objects), and lastly conducted the Morris water maze test (3.3.3) to study spatial navigation and behavioural flexibility in mice.

I considered the first cohort consisting of 3- to 5- months old mice (n = 10 to 11) as the "main" cohort to answer the research question. The second cohort, 10 months old mice (n = 5), was established as a small study to examine if there are behavioural differences between mature adults (cohort 1) and middle aged (cohort2) *Dpy30*ΔH.

3.2.1 Loss of H3K4 methylation results in the presence of anxiety-like behaviour without locomotory deficit

The genotype effect in the first cohort was not significant for the total distance traveled (Figure 6A; $P = 0.317$) and for the average velocity of walking in the open field test (Figure 6B; $P = 0.221$), suggesting that locomotory activities of *Dpy30*ΔH mice were unaffected. However, the *Dpy30*ΔH mice demonstrated anxiety like behaviour. Throughout five minutes of measurement, the animals spent most of the time exploring the peripheral zone of the open field (Figure 6F). There was a significant decrease in the number of crosses into the center arena (one in sixteenth of the entire arena) (Figure 6C; $P = 0.0054$) and the time spent in the center arena (Figure 6D; $P = 0.0037$) in the *Dpy30*ΔH mice compared to the *Dpy30*WT mice.

As seen in the mature adult mice (the cohort1), 10 months old *Dpy30*ΔH mice did not exhibit any sign of locomotory deficit. There were no significant differences in the distance traveled (Figure 7A; $P = 0.257$) and in average velocity between two groups (Figure 7B; $P = 0.128$). The *Dpy30*ΔH mice in cohort 2 also showed anxiety like behaviour as they spent significantly less time in the center arena compared to the *Dpy30*WT litter mates (Figure 7D; $P = 0.0381$). Overall, these results suggest that loss of H3K4me causes anxiety like behaviour but does not affect the horizontal movement in mice.

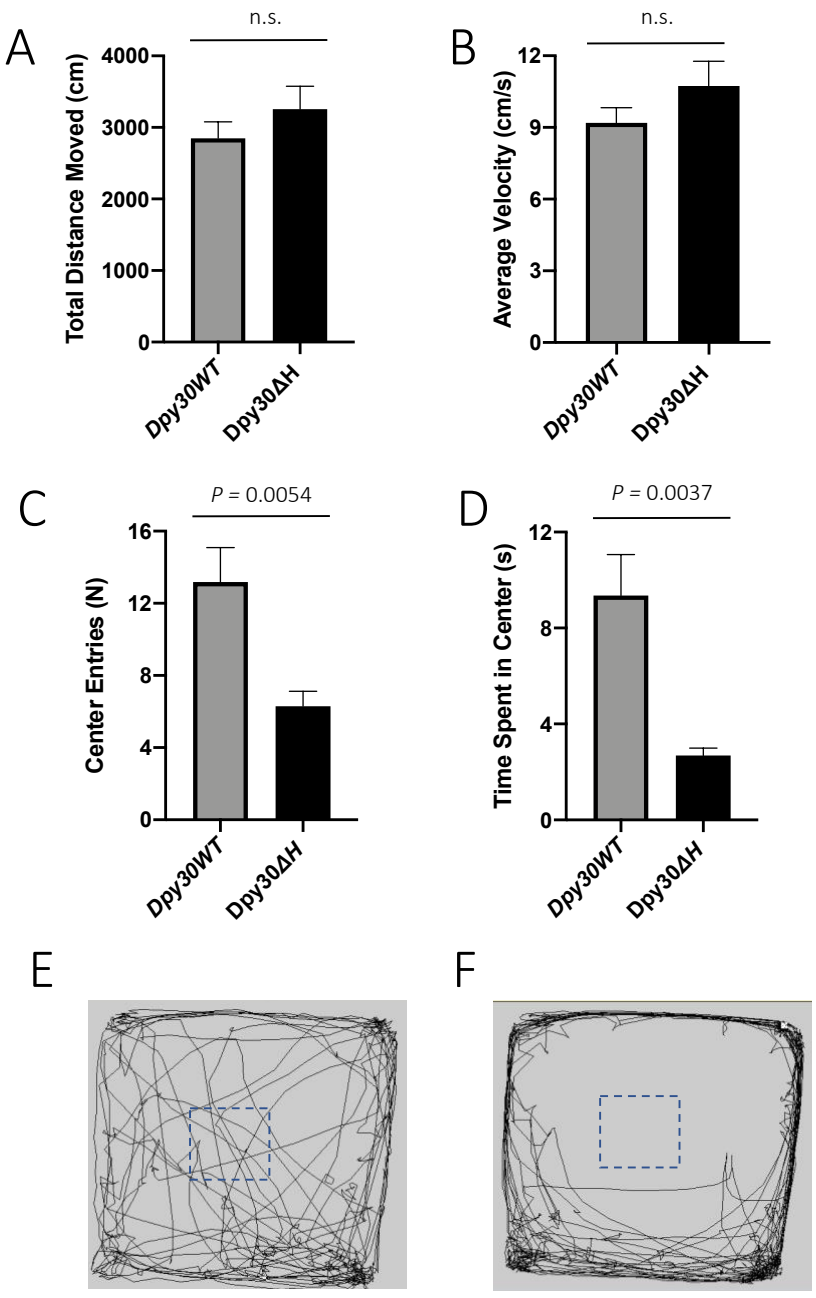

Figure 6: Three to five months old *Dpy30*ΔH mice exhibited anxiety-like behaviour but had normal locomotory coordination in the open field test. (A) Total distance traveled during 5 minutes of measurement [*P*=0.317]. **(B)** Average velocity of walking during 5 minutes of measurement [*P*=0.221]. **(C)** The number of entries to the center arena (1/16) during 5 minutes of measurement**. (D)** Duration of stay in the center arena (1/16) during 5 minutes of measurement. (A-D) Data are presented as mean± SD; unpaired, two-tailed Student's t test with Welch's correction. n.s., not significant. **(E)** Representative traces of walk paths in *Dpy30*WT. **(F)** Representative traces of walk paths in *Dpy30*ΔH.; *Dpy30*WT (n=11) n= *Dpy30*ΔH (n=10)

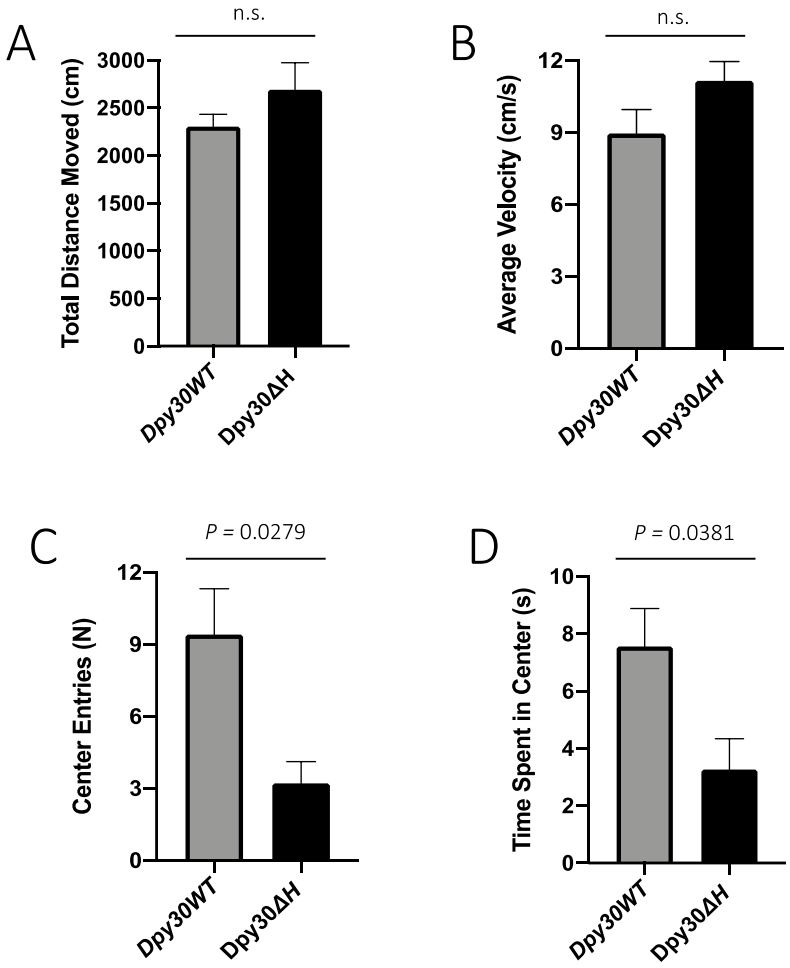

Figure 7: Ten months old *Dpy30*ΔH mice showed anxiety-like behaviour but did not exhibit issues in locomotory coordination in the open field test. (A) Total distance traveled during 5 minutes of measurement [*P*=0.257]. **(B)** Average velocity of walking during 5 minutes of measurement [*P*=0.128]. **(C)** The number of entries to the center arena (1/16) during 5 minutes of measurement**. (D)** Duration of stay in the center arena (1/16) during 5 minutes of measurement.; n = 5/ group (litter mates) Data are presented as mean± SD; unpaired, two-tailed Student's t test with Welch's correction. n.s., not significant.

3.2.2 Loss of H3K4 methylation is associated with impaired recognition memory

*Dpy30*ΔH and *Dpy30*WT mice in both cohorts did not exhibit left and right preference during ten minutes of familiarization training in NORt. There was no significant difference in the number of visits to the left and to the right of the objects (Figure 8A; *Dpy30*ΔH, $P = 0.538$ and *Dpy30*WT, $P = 0.740$). Based on the novelty test, the relative frequency of visiting the novel object was significantly fewer in the *Dpy30*ΔH mice than the *Dpy30*WT mice in both cohort 1 (Figure 8C; $P < 0.0001$) and cohort 2 (Figure 8C; $P < 0.0001$). The *Dpy30*ΔH mice in two cohorts visited the previously exposed "familiar" object more frequently than novel object as the relative frequency was lower than 0.5. Overall, loss of H3K4me cause significant deficits in recognition memory.

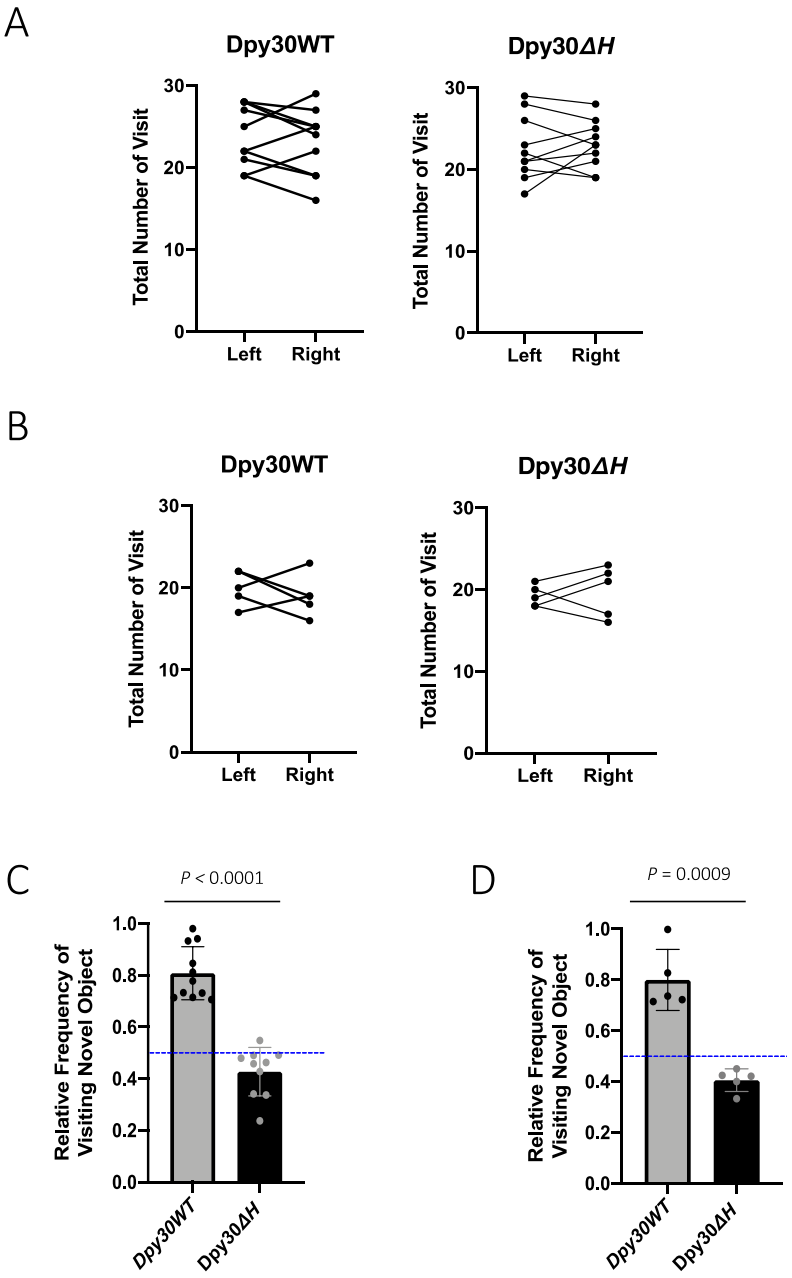

Figure 8: Both three to five months old and ten months old *Dpy30*ΔH mice demonstrated a significant deficit in recognition memory in the novel object recognition test. (A) Left and right preference of objects during 10 minutes of familiarization training in 3 to 5 months old *Dpy30*WT (Left, n=11, *P*=0.740) and *Dpy30*ΔH (Right, n=10, *P*=0.538) mice. **(B)** Left and right preference of objects during 10 minutes of familiarization training in 10 months old *Dpy30*WT (Left, n=5, *P*=0.570) and *Dpy30*ΔH (Right, n=5, *P*=0.602) mice. **(C)** Relative frequency of visiting novel object in 3 to 5 months old *Dpy30*ΔH (n=10) and *Dpy30*WT (n=11) mice. **(D)** Relative frequency of visiting novel object in 10 months old *Dpy30*ΔH and *Dpy30*WT mice (n=5 per group); (A-B) paired, two-tailed Student's t test. (C-D) unpaired, two-tailed Student's t test with Welch's correction. Data are shown as mean ± SD

3.2.3 Loss of H3K4 methylation leads to significant deficit in reversal memory

The acquisition training was performed first to examine the ability of locating a goal platform (spatial navigation) in mice. The hidden platform was located at zone 1 throughout the seven days of measurement (Figure 2B). Latency to locate the escape platform did not differ between the 2 genotypes (Figure 9A; $P = 0.318$). There was a significant improvement in escape latency when compared the first and the seventh day of measurement (Figure 9D; $P < 0.0001$ for both groups). There was no substantial difference in average velocity of traveling throughout the seven days of acquisition training between two groups, which further confirms the absence of locomotory deficit in *Dpy30*ΔH mice (Figure 9B; $P = 0.796$). Twenty-four hours after the acquisition training, the probe test was carried out to examine the formation of spatial memory in mice. Both groups spent a significantly longer duration in the correct quadrant compared to the other three quadrants (Figure 9C; $P < 0.0001$ for both groups). The animals spent least duration in zone 3, diagonal to the correct quadrant.

Following acquisition training, reversal training was completed to determine if mice could re-learn the location of the escape platform when it was moved to the opposite side of the maze (from zone 1 to zone 3). The latency to reach the new location of platform decreased over the first two days of measurements in both groups (Figure 9E; $P = 0.0425$). However, the latency approached an asymptotic level of performance by Day3 in *Dpy30*ΔH mice, while it continued to decrease progressively in *Dpy30*WT mice. There was no substantial difference in escape latency between the first and the last (fifth) day of reversal training in *Dpy30*ΔH mice, suggesting a significant deficit in reversal learning (Figure 9H; $P = 0.0573$). Swimming speed did not differ between the two groups throughout the five days of reversal training, as seen from the acquisition training (Figure 9F; $P = 0.563$). Based on the reversal probe test, I did not

detect a significant bias in the percentage of time *Dpy30*ΔH mice spent in each quadrant (Figure 9G; $P = 0.424$). The animals spent approximately equal duration in each of the four quadrats but spent slightly more time in zone 1 than in zone 3. Subsequently, I calculated the number of entries to the old platform location during reversal training to examine if learning new location of platform interferes with the expression of previously acquired spatial memory (memory extinction) in mice. Remarkably, there was no significant difference in the number of entries to the old platform location between two groups (Figure 9I; $P = 0.879$). *Dpy30*ΔH mice exhibited a gradual decrease in the number of entries to the old platform location, indicating proper memory extinction. I assessed further analysis to examine if release location affects the escape latency, but I did not observe a significant difference between the trial when animals were released close to the hidden platform and the trial when animals were released far from the hidden platform (Figure 11). Lastly, the visible platform test was conducted to determine the extent to which performance in acquisition and reversal training was influenced by non-cognitive confounds, including poor visual ability or reduced motivation to escape from the water. The visible platform was located in zone 2 (Figure 2B). We found that *Dpy30*ΔH mice exhibited similar escape latency time and average swim speed compared with *Dpy30*WT mice, indicating no gross physical impairments in these mice (Figure 10). Taken together, these data indicate that the loss of H3K4me may not be necessary for the acquisition of spatial memory but is required for reversal learning and behavioural flexibility.

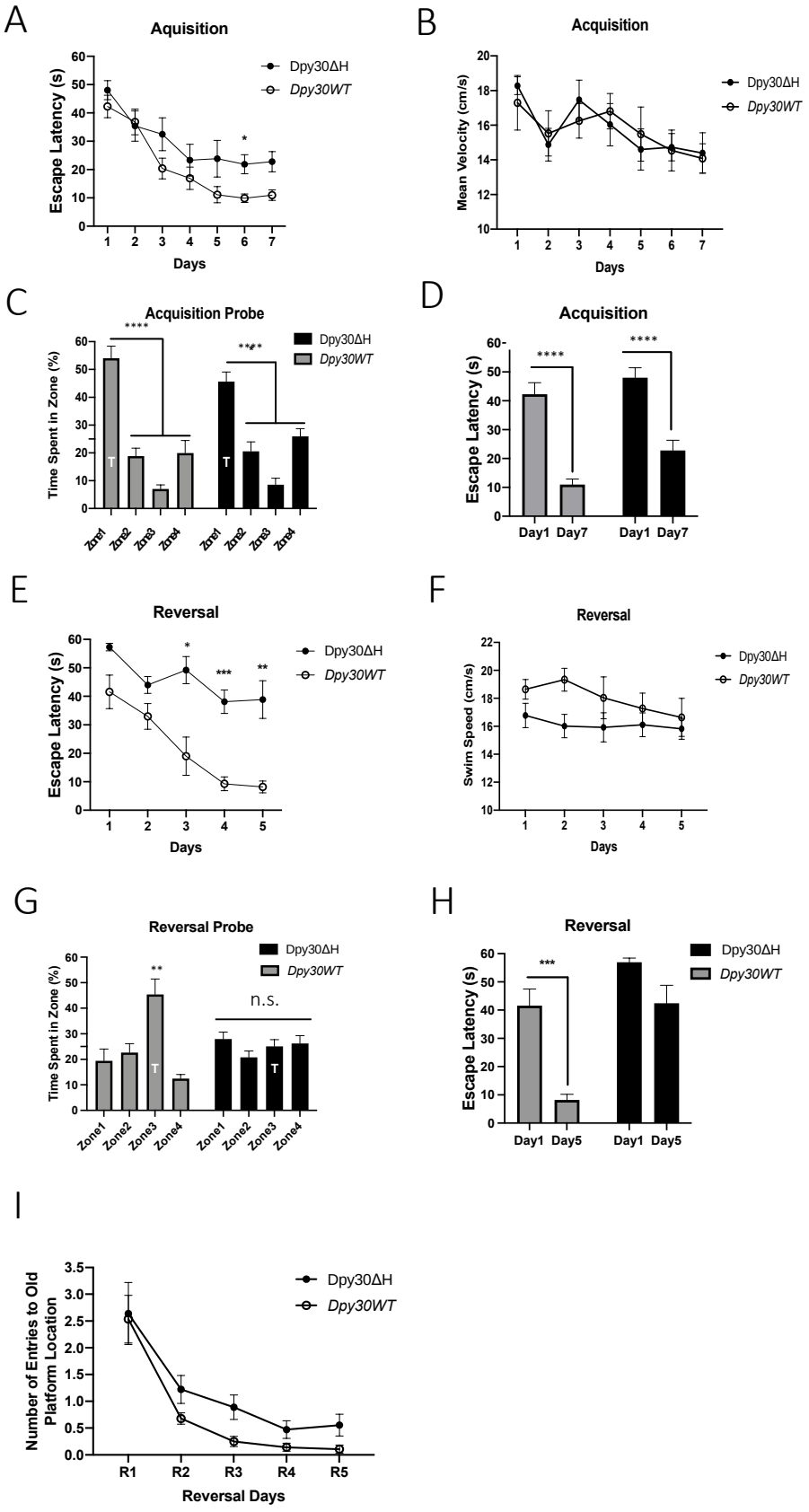
A
Aquisition
Escape Latency (s)
Days
Dpy30ΔH
Dpy30WT
B
Acquisition
Mean Velocity (cm/s)
Days
C
Acquisition Probe
Time Spent in Zone (%)
Zone1
Zone2
Zone3
Zone4
D
Acquisition
Escape Latency (s)
Day1 Day7 Day1 Day7
E
Reversal
Escape Latency (s)
Days
F
Reversal
Swim Speed (cm/s)
Days
G
Reversal Probe
Time Spent in Zone (%)
n.s.
H
Reversal
Escape Latency (s)
Day1 Day5 Day1 Day5
I
Number of Entries to Old Platform Location
R1 R2 R3 R4 R5
Reversal Days

Figure 9: Morris water maze (MWM) study reveals that the loss of H3K4 methylation is significantly associated with reversal learning and behavioural flexibility. (A) Latency to locate the escape platform during acquisition training in 3 to 5 months old *Dpy30*ΔH and *Dpy30*WT mice. [RM ANOVA between genotype and time, P=0.318] **(B)** Average swimming velocity of *Dpy30*ΔH and *Dpy30*WT mice during acquisition training. [RM ANOVA, P=0.796] **(C)** Percentage of time spent in each quadrant in the MWM acquisition probe trial. [one-way ANOVA, zone, P<0.0001 for both]. **(D)** The difference in escape latency between the first and seventh (last) day of acquisition trials in *Dpy30*ΔH and *Dpy30*WT mice. [one-way RM ANOVA, day, P<0.0001 for both] **(E)** Latency to locate the escape platform during reversal training in 3 to 5 months old *Dpy30*ΔH and *Dpy30*WT mice. [RM ANOVA, between genotype and time, P=0.0425] **(F)** Average swimming velocity of *Dpy30*ΔH and *Dpy30*WT mice during reversal training. [RM ANOVA, P=0.563] **(G)** Percentage of time spent in each quadrant in the MWM reversal probe trial. [one-way ANOVA, zone, P=0.0096 (*Dpy30*WT), P=0.424 (*Dpy30*ΔH)] **(H)** The difference in escape latency between the first and fifth (last) day of reversal trials in *Dpy30*ΔH and *Dpy30*WT mice. [one-way RM ANOVA, P=0.0003 (*Dpy30*WT), P=0.0573 (*Dpy30*ΔH)] **(I)** The number of entries to old platform location in *Dpy30*ΔH and *Dpy30*WT mice. [RM ANOVA, between day and genotype, P=0.879]; *Dpy30*ΔH (n=10), *Dpy30*WT (n=11), Data is shown as mean ± SEM. Bonferroni post hoc analysis was used for ANOVA. *P< 0.05, ****P < 0.0001 [ANOVA within days], n.s. not significant

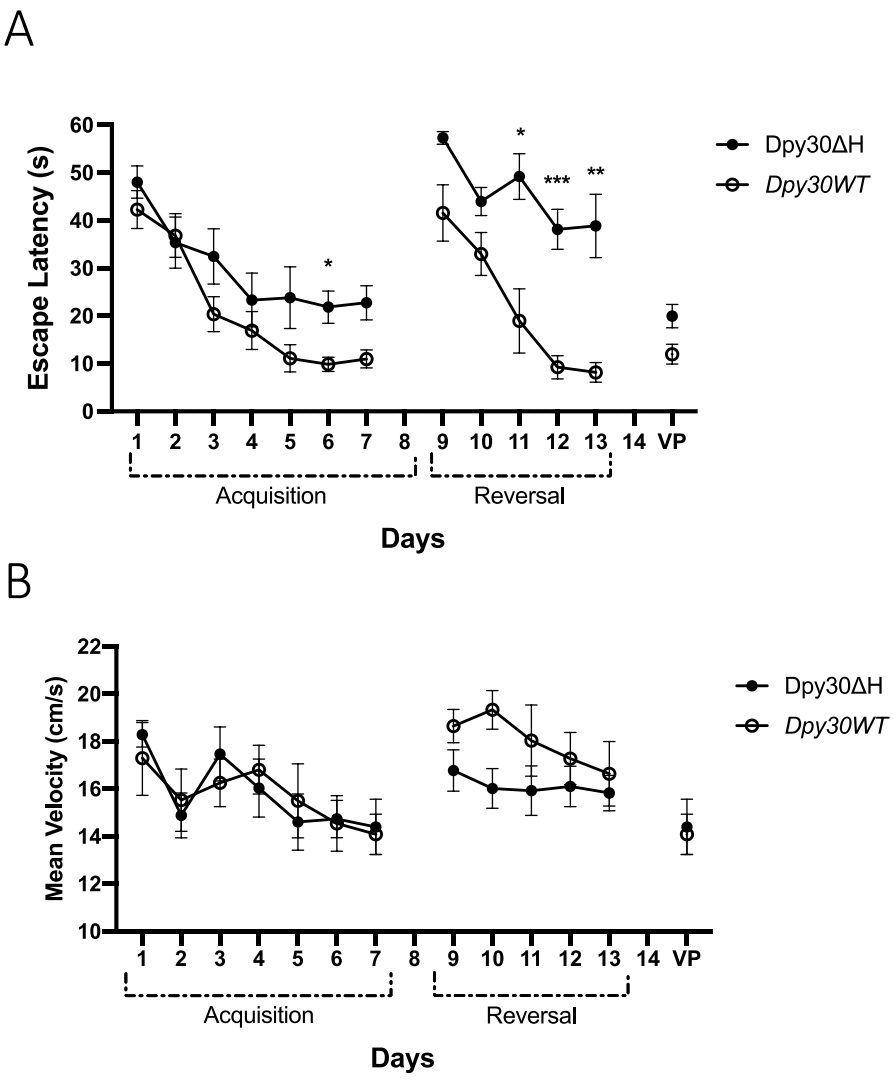

Figure 10: Escape latency and average swimming speed of three to five months old *Dpy30*ΔH and *Dpy30*WT mice throughout fifteen consecutive days of Morris water maze experiment. (A) Latency to locate the escape platform. [RM ANOVA, between day and genotype, *P*=0.318 (Acquisition), *P*=0.0425 (Reversal)] **(B)** Average swimming velocity. [not significant between day and genotype, *P*=0.796 (Acquisition), *P*=0.563 (Reversal)]; Probe tests were conducted on Day8 and on Day14. VP indicates visual platform test, performed Day 15 (last day) of MWM test. *Dpy30*ΔH (n=10), *Dpy30*WT (n=11), Data are shown as mean ± SEM. Bonferroni's post hoc analysis. **P* < 0.05, ***P* < 0.01, ****P* < 0.001 [ANOVA within days]

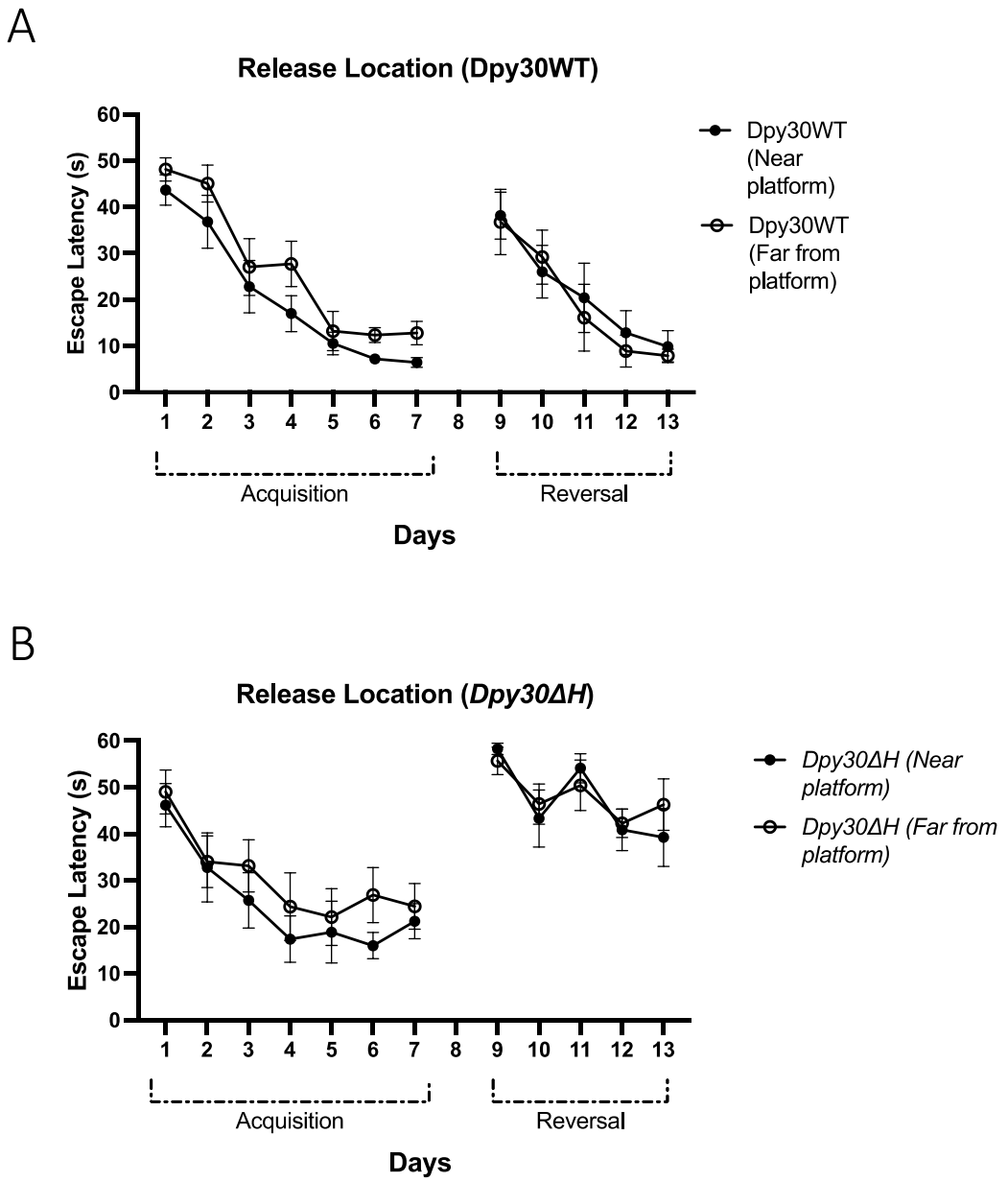

Figure 11: Morris water maze (MWM) study reveals that release location does not affect escape latency. (A) Latency to locate the escape platform in 3 to 5 months old *Dpy30*WT mice (n=11) when released near or far from platform. [RM ANOVA, release location, *P*=0.882] **(B)** Latency to locate the escape platform in 3 to 5 months old *Dpy30*ΔH (n=10) mice when released near or far from platform. [RM ANOVA, release location, *P*=0.362] Releasing from north (N) or from west (W) is considered as close to platform during acquisition training but far from platform during reversal training. Releasing from south (S) or from east (E) is considered as far from platform during acquisition training but close to platform during reversal training. Data is shown as mean ± SEM.

3.3 The level of H3K4 methylation is reduced in the hippocampus of Alzheimer's disease

Prior to the human donor study, I assessed the level of H3K4 methylation in the CA1 pyramidal region of hippocampus on the rodent Alzheimer's disease (AD) model, 5XFAD, and the littermate control mice. The sample collection was done at 9 months of age because the model was designed to develop amyloid plaques spreading through the whole hippocampus, leading to neuronal loss in the mice around the age. Based on the histology work, immunofluorescent intensity of H3K4me3 appeared to be lower in the nine-months old 5XFAD mice compared to the control mice (Figure 12A). Next, I performed immunoblotting analysis of the hippocampus from the AD donors and from the healthy control (n=10 each). Remarkably, the level of H3K4me3 was significantly lower in the hippocampus of AD sample (Figure 12C; $P = 0.0009$), whereas no difference was seen for H3K4me1 (Figure 12D; $P = 0.857$).

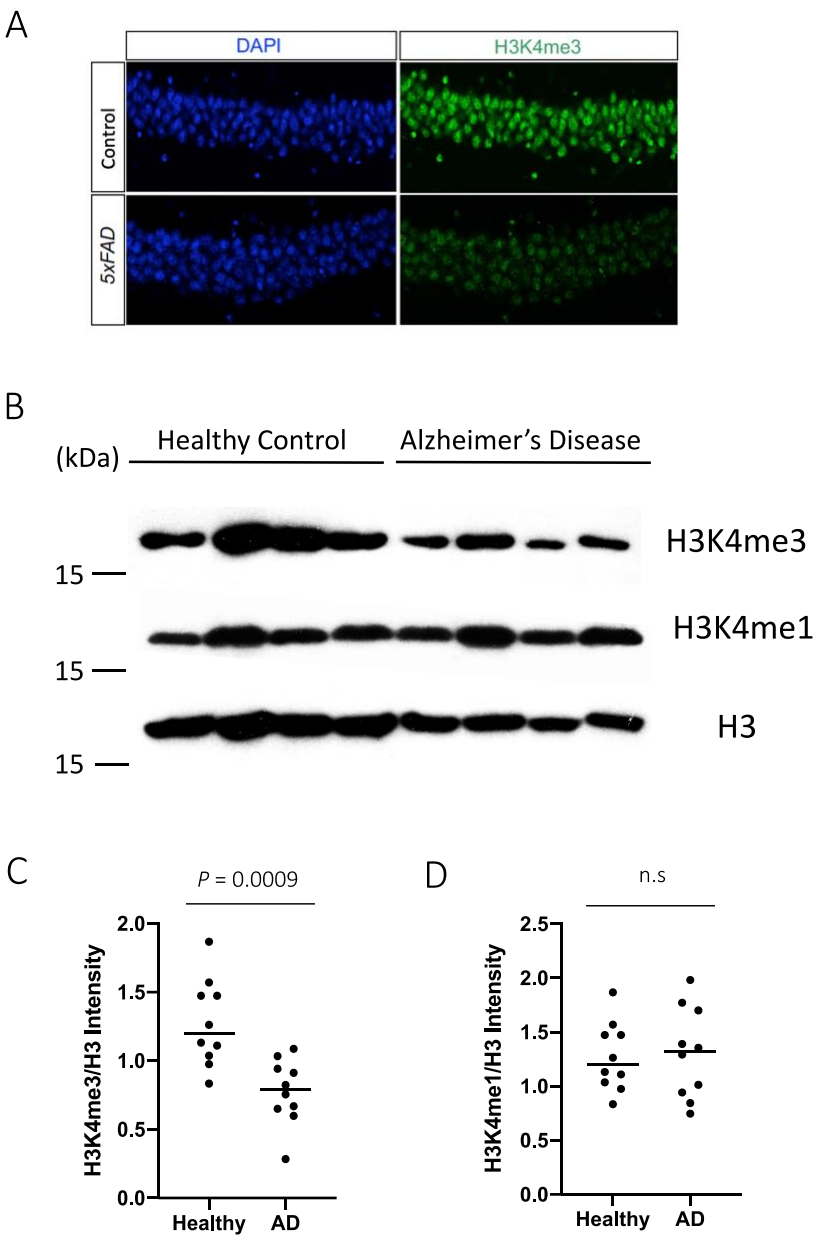

Figure 12: Altered characteristics of H3K4 methylation in Alzheimer's disease. (A) Immunofluorescent imaging of Dapi (blue) and H3K4me3 (green) in the CA1 pyramidal neurons of B6SJ control (top) and that of 5XFAD mice (bottom) at 9 months of age. **(B)** Immunoblot of H3K4me3, H3K4me1, and total H3 in the hippocampus from Alzheimer's disease and control donors. **(C)** Column dot graph indicating H3 normalized H3K4me3 band intensity in Alzheimer's disease and healthy frozen hippocampal samples. **(D)** Column dot graph indicating H3 normalized H3K4me1 band intensity in Alzheimer's disease and healthy frozen hippocampal samples. Data presented as mean with values from individual donors; Alzheimer's disease donors (n=10), healthy control donors (n=10). *P*-value was calculated by unpaired student t test with Welch's correction. n.s., not significant (*P*=0.857).

Chapter 4: Discussion

4.1 Validity of *Dpy30*ΔH mouse model

H3K4 tri-methylation (H3K4me3) is highly enriched at active promoters. It is extensively regulated throughout development and aging [11,50]. Dynamic regulation of H3K4me3 is critical for cognitive processing and its dis-regulation is linked to neuropsychiatric disorders, such as schizophrenia and a plethora of intellectual disability syndrome [51,52]. To date, there are at least six H3K4 specific KMTs identified in the mammalian cells. All six KMTs are strongly expressed in the hippocampus throughout the human life span, indicating their potential contribution to hippocampal synaptic plasticity. In fact, hippocampal specific *Kmt2a* (*Mll1*) and or *Kmt2b* (*Mll2*) knockout mice display anxiety-like behaviour and have impaired spatial navigation [30,31]. Furthermore, deletion of *Kmt2a* in the adult prefrontal cortex causes significant deficits in spatial working memory with severely impaired short-term plasticity in mice [53]. Nonetheless, as noted earlier, KMT2A and KMT2B have co-activator functions that have a larger influence on gene expression than does their catalytic activity [32,34,35]. As such, the specific role of H3K4me in the hippocampal function remains unclear.

Our previous studies have demonstrated that deletion of *Dpy30*, which is essential for the catalytic activity of all six TrxG complexes *in vivo*, but not their assembly or co-activator functions in the developing pancreas, has minimal effect on gene expression [54,45]. However, the activation of a subset of genes with critical roles in pancreatic acinar cell maturation and function was severely compromised [32]. Based on these data, I hypothesize that H3K4me is not required to maintain the expression of most genes but is important for the activation of a subset of cell-type specific genes critical in maintaining cell-specific functions. Hence, to begin

to examine what role H3K4me plays in the normal function of hippocampal neurons, we have disrupted *Dpy30* in the hippocampus of adult mice, using a Camk2a-Cre; *Dpy30*$^{flox/flox}$; tdTomato^{+} model (*Dpy30*ΔH).

In my study, *Camk2a-Cre* was selected as a Cre driver because it is primarily expressed in the CA1 pyramidal cell layers of hippocampus in mice after the third postnatal week [45]. This regionally- and temporally- restricted gene deletion does not require inducing agents, like tamoxifen. Moreover, the lack of activity of *Camk2a* promoter during early brain development is expected to reduce the possibility of developmental defects caused by deletion of *Dpy30*, allowing more precise interpretation of gene function in the adulthood. I have confirmed that DPY30 protein is significantly deleted in the CA1 pyramidal neurons of *Dpy30*ΔH mice by 2 months of age (Figure 3). Significant loss of H3K4me is delayed to 3 months of age in *Dpy30*ΔH mice (Figure 4). This delay in reduction of H3K4me is considered due to slow turnover of histone protein [55]. In general, histones with active markers have a faster turnover rates than those with silent marks. However, histone proteins involved in bivalent chromatin (H3K4me3/H3K27me3) have slower turnover rates than histone proteins with either mark alone. Furthermore, DPY30-positive neurons in the 3-months-old *Dpy30*ΔH mice do not express *tdTomato*, which further confirms the specificity of Cre-loxP recombination in this model. Subsequently, I have examined whether the loss of *Dpy30* affected level of neurogenesis and gross anatomy of hippocampus because morphological abnormalities could potentially become confounding variables, affecting neuronal communication within hippocampus and to other brain regions. Nonetheless, hippocampal neurogenesis and morphology appeared to be unaffected in the model (Figure 5.)

4.2 Loss of H3K4 methylation does not affect motor coordination in mice.

In support of H3K4 methylation playing a critical role in neurons, disruption of *Dpy30* in mouse NSCs impairs the differentiation of neuronal and glial lineages [56]. However, these mice could not survive after P27 due to defective postnatal brain development. Therefore, the effects of H3K4me reductions on the hippocampus-dependent behaviour and memory formation have not been investigated. We, on the other hand, disrupted *Dpy30* in post-mitotic pyramidal neurons of the hippocampus of adult mice, using *Camk2a-Cre*. Therefore, I could focus on the effect of H3K4me reduction in the intellectual properties of mice. I assessed a series of behavioural batteries, including open field test (OF), novel object recognition test (NORt), and the Morris water maze test (MWM) in order to examine both cognitive and physiological abilities of mice. Based on all three behavioural experiments, hippocampal neuronal loss of H3K4me did not affect locomotory coordination in mice. There were no significant differences in the distance traveled and the average velocity of walking (Figure 6 and Figure 7). The results were somewhat anticipated since motor coordination is not part of hippocampal functions.

4.3 Loss of H3K4 methylation results in the development of anxiety-like behaviour in mice.

The *Dpy30*ΔH mice spent a significantly shorter duration in the center arena (1/16 of entire arena) compared to the *Dpy30*WT mice, indicating anxiety-like behaviour in the *Dpy30*ΔH mice. I did not observe age-related difference in anxiety-like behaviour (Figure 6 and Figure 7). Further work is necessary to understand the contribution of H3K4me to gene regulatory mechanism governing anxiety-like behaviour. I would expect that transcriptional

activation of genes regulating neural inputs arising from the ventral hippocampus (vHF) to the medial prefrontal cortex (mPFC) and the lateral septum (LS) would be affected due to the loss of H3K4me [57]. There are functional differences between dorsal and ventral hippocampus. The dorsal hippocampus (dHF) is responsible for cognitive processing, such as spatial learning and memory [37,38]. It receives visual and spatial information from the anterior cingulate and retrosplenial cortices via the medial entorhinal cortex. The vHF, on the other hand, has major connections with the prefrontal cortex, amygdala, and hypothalamus, and is involved in emotional processing, such as anxiety. Recent studies have shown that anxiety-like behaviours are modulated in a bidirectional manner [58]. Glutamatergic firing of mPFC-projecting vHF cells is responsible for the increase in anxiety while inhibition of these cells helps to decrease anxiety. Conversely, activation of LS-projecting vHF cells is responsible for the decrease in anxiety, whereas inhibition of these cells produces anxiety promoting effects. Anxiety is an adaptive response to help animals from potential life-threatening situations. When animals are exposed to anxiety-provoking environment like OF, there is an increase in firing from vHF neurons projecting to the mPFC, which provokes anxiety-like behaviour [59,60]. Compared to anxiety-promoting role, the anxiolytic function of the vHF is less understood. LS is thought to be an intermediate structure connecting the vHF to the paraventricular hypothalamus, thereby activating hypothalamus-pituitary-adrenal (HPA) axis to cope with anxiety-related stress. Nonetheless, H3K4me may be associated with hyper-activation of mPFC-projecting vHF cells or potentially be involved in the inhibition of LS-projecting vHF cells.

4.4 Loss of H3K4 methylation leads to impaired recognition memory.

The novel object recognition test (NORt) is a behavioural assay commonly used to evaluate cognition, particularly recognition memory [61]. This study relies on the innate preference of rodents for novelty. Lego blocks and 50ml falcon tubes containing colored pencils were randomly assigned to each animal in order to avoid the potential effect of confounding variables, such as shape and appearance of object. Moreover, the designation of the novel object and its left or right position is counterbalanced to avoid preference for location. There were no significant differences in the number of visits to the left and to the right of the objects during the familiarization step, suggesting the absence of location preference both in *Dpy30*ΔH and *Dpy30*WT mice (Figure 8). Based on the novelty test, the relative frequency of visiting the novel object was significantly lower in *Dpy30*ΔH mice than *Dpy30*WT mice. The *Dpy30*ΔH mice visited "familiar" object more frequently than the novel object, which further indicates impaired recognition memory in *Dpy30*ΔH mice.

Recognition memory refers to the ability to identify the previously encountered events, objects, or people. The two components of recognition memory are recollection of the stimulus in the context of other information (e.g. spatial and temporal) associated with the experience, and the judgment of familiarity with the stimulus. Some of the previous studies have addressed that the hippocampus is responsible for recollection, but not familiarity [62,63], while other studies indicated that the hippocampus is critical for both recollection and familiarity [64,65]. One of the evidences for the hippocampal contribution to familiarity is a significant increase in extracellular dHF glutamate efflux after mice were exposed to familiar object twice (second familiarization steps) [66]. Nonetheless, further research can build on these findings by investigating if H3K4me is critical for recollection and/or familiarity.

4.5 Loss of H3K4 methylation has a minor effect on spatial memory acquisition but results in significant reversal memory deficit.

During acquisition training, latency to locate the escape platform did not differ between *Dpy30*ΔH and *Dpy30*WT mice (Figure 9A-D). There was a significant improvement in escape latency from the first to the seventh (last) day of acquisition measurement. These data suggest that loss of H3K4me has minimum effect on acquisition of spatial memory. However, when it comes to reversal memory, *Dpy30*ΔH mice did not show much progress in escape latency (Figure 9E-H). By the third day of reversal training, the latency approached an asymptotic level of performance in *Dpy30*ΔH mice. A significant bias in the percentage of time *Dpy30*ΔH mice spent in each quadrant was not detected according to the reversal probe test. The animals spent approximately equal duration in each of the four quadrats but spent slightly more time in zone 1 than in zone 3. Hence, I hypothesized that learning new location of platform does not hinder the expression of previously acquired spatial memory (impaired memory extinction) in the *Dpy30*ΔH mice. However, the animals appeared to have proper memory extinction, as revealed by gradual decrease in the number of entries to the old platform location. I assessed further analysis to examine if release location affects escape latency, but I did not observe a significant difference between the trial when animals were released close to the hidden platform and the trial when animals were released far from the hidden platform. Future efforts have to be made in order for better understanding of mechanism underlying a significant impairment in reversal memory with proper memory extinction.

4.6 There was a significant reduction of H3K4me3 in the hippocampus of Alzheimer's disease.

As noted earlier, both rodent Alzheimer's disease (AD) model and hippocampal specific *Kmt2a* knockout model shared similar alterations in gene expression; H3K4me3 is increased at inflammatory genes while is decreased at genes involved in learning and memory [31,43]. The evidence comes from humans is even less. H3K4me3 was significantly less in the nucleus but rather was abnormally increased in the cytoplasm of the hippocampus of AD patients [44]. From these data, I hypothesize that the loss of H3K4me in hippocampal neurons is part of the pathogenesis of AD, which may contribute to cognitive impairment appeared in the disease. To test this hypothesis, I examined if level of H3K4me is altered in the hippocampus of rodent AD model and in the hippocampus of human AD samples. The 5XFAD (Tg6799) model was selected for this study because it contains five human familial AD gene mutations, including APP mutations from the Swedish, Florida and London families, along with two mutations in presenilin-1 [48]. This model appeared to be superior representation of human disease over other AD models without human originated genes like CK-p25 model. It is designed to rapidly recapitulate a portion of the pathological alterations present in the human AD. Intraneuronal Ab starts to rapidly accumulate in the brain of 5XFAD at 1.5 months of age. The animals begin to show impaired spatial working memory around 4 months old. Amyloid plaques cover up the whole hippocampus and cortex at 6 months, which eventually leads to neuronal loss in the mice by 9 months of age. Based on the histological analysis, the intensity of H3K4me3 appeared to be lower in the CA1 region of hippocampus in the 5XFAD than age-matched control mice (Figure 12). The immunoblot analysis of AD donor samples supported the rodent histology results and showed a significant decrease in H3K4me3 in the hippocampus of AD

compared to the healthy control. On the other hand, no difference was seen for H3K4me1. Monomethylation of H3K4 is predominantly associated with active and poised enhancers and distinguishes the boundaries of active promoters, thus limiting the recruitment of transcription factors [67]. Taken together, histological and immunoblot analysis provided evidence of altered H3K4me in the hippocampus of AD.

Some limitations involved in the AD project are inadequate amount and quality of AD data. Highly accumulated Ab and tau proteins in the 5XFAD brain interfere antigen-antibody interaction, making it difficult to analyze histological data. The nuclear marker Dapi was employed as a reference to determine the fluorescence intensity of H3K4me3 in 5XFAD and in control CA1 pyramidal hippocampal neurons. Optimization of histology protocol, such as introducing clearing step, would be required to improve quality of staining and to determine statistical significance of the results. Furthermore, there is a limitation in the sample selection for post-mortem brain study. Age- and sex-matched CA1 pyramidal layer of hippocampus from the AD and healthy control donors were requested to the brain bank. While a histopathological verification has been made, anatomic specificity and the sample quality was not evaluated during a process of tissue sampling. In order to examine the level of H3K4me within neuronal population, histological analysis using cell type-specific antibodies would be favoured methodology over immunoblot analysis. Nonetheless, I believe that data presented in this study help expand our understanding of the role of H3K4me in hippocampal memory formation.

4.7 Significance and future directions

My findings indicate that H3K4 methylation (H3K4me) is involved in the transcriptional regulation of hippocampal memory processing. Experimental loss of H3K4me in the hippocampal excitatory neurons results in the development of anxiety-like behaviour and is associated with impaired recognition and reversal memory in mice. The *Dpy30*ΔH mice generated in this study is considered as more appropriate model to study *in vivo* function of H3K4me than previous KMTs knockout model [30,31]. Deletion of *Dpy30* inhibits methylation of H3K4 while it still allows an assembly of TrxG complex, thereby harbouring a potential to regulate gene expression through enzyme-independent function such as binding to other TFs. Hence, data presented in this study are more meaningful than previous studies where there was uncertainty in the experimental variable; loss of H3K4me or loss of co-activator function.

The highest priority of future research would be a collection of molecular data. My project originally aimed to investigate if H3K4me is required for transcriptional activation of memory-associated genes in the hippocampus. To test this hypothesis, I planned to conduct bulk RNA sequencing and to assess the differential gene expression between *Dpy30*ΔH and *Dpy30*WT mice. In order to perform RNA-seq, it is necessary to isolate Cre-positive nuclei or potentially neurons from the brain samples. However, the dissociation of neuronal nucleic or cell suspension from the adult mouse brain is extremely challenging compared to that from embryonic mouse brain or from cell culture. The axons in adult brain are highly myelinated with the growing complexity of the nervous system [68]. Notably, myelin sheath has an intrinsic fluorescence property, which may interfere with gating of fluorescent markers (e.g. tdTomato) during fluorescence-activated cell sorting (FACs) [69]. An immediate future work

would be optimization of neuron dissociation protocol to further elucidate the cellular and biological mechanisms underlying transcriptional regulation of hippocampal memory formation.

4.8 Overall conclusions

Although it is increasingly clear that H3K4 methylation plays a critical role in the hippocampal neuronal communication, little is known about the transcriptional contribution of H3K4 methylation to the hippocampal memory processing. As the first step, this project aimed to investigate whether the loss of H3K4 methylation affects proper consolidation of hippocampal memory. Overall, data presented in this thesis demonstrate that H3K4 methylation is required for hippocampal function, such as managing anxiety, and proper formations of recognition and reversal memory. Furthermore, the immunoblot analysis of human patient samples indicates altered H3K4 methylation in the Alzheimer's disease. Collectively, I hope these findings help shed light on H3K4 methylation as a potential contributor to establish a therapeutic intervention for the cognitive decline associated with the disease.

References

1. Jinno, S. and Kosaka, T. (2010) Stereological estimation of numerical densities of glutamatergic principal neurons in the mouse hippocampus. *Hippocampus,* 20:829-840
2. Andersen, P. *et al.* (2007) *The Hippocampus Book.* Oxford: Oxford University Press
3. Vinogradova, O.S. (2001) Hippocampus as comparator: role of the two input and two output systems of the hippocampus in selection and registration of information. *Hippocampus.* 11(5):578-598
4. Zhang, X.M. and Zhu, J. (2011) Kainic acid-induced neurotoxicity: targeting glial responses and glia-derived cytokins. *Curr Neuro Pharm.* 9(2):388-398
5. Hasselmo, M.E. (2000) A cortical-hippocampal system for declarative memory. *Nat Rev Neuro.* 1:41-50
6. Scoville, W.B. and Milner, B. (1957) Loss of recent memory after bilateral hippocampal lesions. *J Neurol Neurosurg Psychiatry.* 20(1):11–21
7. Squire, L.R. (1992) Memory and the hippocampus: a synthesis from findings with rats, monkeys, and humans. *Psychol Rev.* 99:195–231
8. O'Keefe, J. and Dostrovsky, J. (1971) The hippocampus as a spatial map. Preliminary evidence from unit activity in the freely-moving rat. *Brain Res.* 34:171–175
9. Bannerman, D.M. *et al.* (2004) Regional dissociations within the hippocampus – memory and anxiety. *Neurosci Biobehav Rev.* 28(3):273-283
10. Pelkey, K.A. *et al.* (2017) Hippocampal GABAergic inhibitory interneurons. *Physiol Rev.* 97:1619e1747
11. Guenther, M.G. *et al.* (2007) A chromatin landmark and transcription initiation at most promoters in human cells. *Cell.* 130:77–88
12. Choy, J.S. *et al.* (2010) DNA methylation increases nucleosome compaction and rigidity. *J Am Chem Soc* 132:1782–1783.
13. Teissandier, A. and Bourc'his, D. (2017) Gene body DNA methylation conspires with H3K36me3 to preclude aberrant transcription. *EMBO J* 36:1471–1473
14. Tate, P.H. and Bird, P. (1993) Effects of DNA methylation on DNA-binding proteins and gene expression. *Curr Opin Genet Dev* 3:226–231
15. Stirzaker C. *et al.* (2017) Methyl-CpG-binding protein MBD2 plays a key role in maintenance and spread of DNA methylation at CpG islands and shores in cancer. *Oncogene* 36:1328–1338.
16. Fuso, A. (2012) Chapter 26: Aging and disease: the epigenetic bridge, *Epigenetics in Human Disease*, 519-544
17. Miller, C.A. *et al.* (2010) Cortical DNA methylation maintains remote memory. Nature *Neuro Sci.* 13:664-666

18. Levenson J.M. *et al.* (2006) Evidence that DNA (cytosine-5) methyltransferase regulates synaptic plasticity in the hippocampus. *Journal of Biological Chemistry*, 281:15763–15773

19. Lipsky, R.H. (2013) Epigenetic mechanisms regulating learning and long-term memory. *International Journal of Developmental Neuroscience*, 31(6):353-358

20. Levenson, J.M. *et al.* (2004) Regulation of histone acetylation during memory formation in the hippocampus. *Journal of Biological Chemistry*, 279(39): 40545–59

21. Johansen, J.P. *et al.* (2011) Molecular mechanisms of fear learning and memory. *Cell*, 147: 509–24

22. Wang, Z. *et al.* (2008) Combinatorial patterns of histone acetylations and methylations in the human genome. *Nat Genet.* 40:897–903

23. Schwartz, Y. B. and Pirrotta, V. (2007) Polycomb silencing mechanisms and the management of genomic programmes. *Nat Rev Genet*. 8:9–22

24. Gupta, S. *et al.* (2010) Histone Methylation Regulates Memory Formation. *J of Neurosci*. 30:3589–3599

25. Schuettengruber, B. *et al.* (2007) Genome regulation by polycomb and trithorax proteins. *Cell.* 128:735–745

26. Shilatifard, A. (2012). The COMPASS family of histone H3K4 methylases: mechanisms of regulation in development and disease pathogenesis. *Annu Rev Biochem*. 81:65–95

27. Hyun, K. *et al.* (2017) Writing, erasing and reading histone lysine methylation. *Exp. Mol.* 49 e324

28. Bochyńska, A. *et al.* (2018) Modes of interaction of KMT2 histone H3lysine 4 methyltransferase/COMPASS complexes with chromatin. *Cells.* 7

29. Benito, E. *et al.* (2015) HDAC inhibitor-dependent transcriptome and memory reinstatement in cognitive decline models. *Journal of Clinical Investigation*, 125(9):3572–3584

30. Kerimoglu, C. *et al.* (2013) Histone-methyltransferase MLL2 (KMT2B) is required for memory formation in mice. *J of Neurosci*, 33(8):3452-3464

31. Kerimoglu, C. *et al.* (2017) KMT2A and KMT2B mediate memory function by affecting distinct genomic regions. *Cell Reports*, 20:538-548

32. Campbell, S. A. *et al.* (2019) TrxG Complex Catalytic and Non-catalytic Activity Play Distinct Roles in Pancreas Progenitor Specification and Differentiation. *Cell Reports.* 28: 1830–1844

33. Sze, C. C. *et al.* (2017) Histone H3K4 methylation-dependent and -independent functions of Set1A/COMPASS in embryonic stem cell self-renewal and differentiation. *Genes & Development.* 1732–1737

34. Dorighi, K. M. *et al.* (2017) Mll3 and Mll4 Facilitate Enhancer RNA Synthesis and Transcription from Promoters Independently of H3K4 Monomethylation. *Mol Cell.* 66(4):568-576

35. Rickels, R. *et al.* (2017) Histone H3K4 monomethylation catalyzed by Trr and mammalian COMPASS-like proteins at enhancers is dispensable for development and viability. *Nature Genet.* 49:1647–1653

36. Hödl, M. and Basler, K. (2012) Transcription in the absence of histone H3.2 and H3K4 methylation. *Curr Biol.* 22(23):2253-2257

37. Burns, A. and Iliffe, S. (2009) Alzheimer's disease. *BMJ*. 338:b158

38. Braak, H. and Braak, E. (1991) Neuropathological staging of Alzheimer-related changes. *Acta Neuropathologica*. 82:239-259

39. Masukar, A. (2018) Towards a circuit-level understanding of hippocampal CA1 dysfunction in Alzheimer's disease across anatomical axes. *J Alzheimers Dis Parkinsonism*. 8(1):412

40. Jones, W.D. *et al.* (2012) De novo mutations in MLL cause wiedemann-steiner syndrome. *Am J Hum Genet.* 91:358–64

41. Dong, S. *et al.* (2014) De novo insertions and deletions of predominantly paternal origin are associated with autism spectrum disorder. *Cell Rep.* 9:16–23

42. Najmabadi, H. *et al.* (2011) Deep sequencing reveals 50 novel genes for recessive cognitive disorders. *Nature.* 478:57–63

43. Gjoneska, E. *et al.* (2015) Conserved epigenomic signals in mice and humans reveal immune basis of Alzheimer's disease. *Nature.* 518(7539):365-9

44. Mastroeni, D. *et al.* (2015). Aberrant intracellular localization of H3K4me3 demonstrates an early epigenetic phenomenon in Alzheimer's disease. *Neurobiol. Aging.* 36:3121–3129

45. Haddad, J. *et al.* (2018) Structural analysis of the Ash2L/Dpy-30 complex reveals a heterogeneity in H3K4 methylation. *Structure.* 26:1567-1570

46. Patel, R. *et al.* (2011) A novel non-SET domain mullti-subunit methyltransferase required for sequential nucleosomal histone H3 methylation by the mixed lineage leukemia protein-1 (MLL1) core complex. *J. Biol. Chem.* 286:3359-3369

47. Wang, Q. *et al.* (2014). Arcuate AgRP neurons mediate orexigenic and glucoregulatory actions of ghrelin. *Molecular metabolism*, *3*(1), 64-72.

48. Oakley, H. *et al.* (2006) Intraneuronal beta-amyloid aggregates, neurodegeneration, and neuron loss in transgenic mice with five familial Alzheimer's disease mutations: potential factors in amyloid plaque formation. *J of Neuro.* 26(40):10129-10140

49. Tsien, J.Z. *et al.* (1996) Subregion- and cell type-restricted gene knockout in mouse brain. *Cell.* 87:1317-1326

50. Barrera, L.O. *et al.* (2008) Genome-wide mapping and analysis of active promoters in mouse embryonic stem cells and adult organs. *Genome Res.* 18:46–59

51. Shen, E. *et al.* (2014) Regulation of histone H3K4 methylation in brain development and disease. *Philos Trans R Soc Lond B Biol Sci.* 369:20130514

52. Takata, A. *et al.* (2014) Loss-of-function variants in schizophrenia risk and SETD1A as a candidate susceptibility gene. *Neuron.* 82:773–780

53. Jakovcevski, M. *et al.* (2015) Neuronal Kmt2a/Mll1 histone methyltransferase is essential for prefrontal synaptic plasticity and working memory. *J of Neurosci.* 35(13):5097-5108

54. Dilworth, D. and Arrowsmith, C.H. (2018) Guiding COMPASS: Dpy-30 positions SET1/MLL epigenetic signaling. *Structure.* 26(12):1567-1570

55. Zee, B. *et al.* (2010) Global turnover of histone post-translational modifications and variants in human cells. *Epigenetics and Chromatin.* 3(1):1-11

56. Shah, K., King, G.D. and Jiang, H. (2019) A chromatin modulator sustains self-renewal and enables differentiation of postnatal neural stem and progenitor cells. *J Mol Cell Biol.* 12(1):4-16

57. Parfitt, G.M. *et al.* (2017) Bidirectional control of anxiety-related behaviours in mice: role of inputs arising from the ventral hippocampus to the lateral septum and medial prefrontal cortex. *Neuropsychopharmacology.* 42:1715-1729

58. Parfitt, G.M., Nguyen, R., Bang, J.Y. *et al.* (2017) Bidirectional control of anxiety-related behaviours in mice: role of inputs arising from the ventral hippocampus to the lateral septum and medial prefrontal cortex. *Neuropsychopharmacology.* 42:1715-1729

59. Adhikari A, Topiwala MA, Gordon JA (2010). Synchronized activity between the ventral hippocampus and the medial prefrontal cortex during anxiety. *Neuron.* 65: 257–269.

60. Adhikari A, Topiwala MA, Gordon JA (2011). Single units in the medial prefrontal cortex with anxiety-related firing patterns are preferentially influenced by ventral hippocampal activity. *Neuron.* 71: 898–910

61. Broadbent, N.J. *et al.* (2010) Object recognition memory and the rodent hippocampus. *Learn Mem.* 17:5-11

62. Montaldi, D. and Mayes, A.R. (2010) The role of recollection and familiarity in the functional differentiation of the medial temporal lobes. *Hippocampus.* 20:1291-1314

63. Yonellinas, A.P. (2001) Components of episodic memory: the contribution of recollection and familiarity. *Philos. Transcr.* 356:1363-1374

64. Broadbent, N.J. *et al.* (2010) Object recognition memory and the rodent hippocampus. *Learn. Mem.* 17:5-11

65. de Lima, M.N. *et al.* (2006) Temporary inactivation reveals an essential role of the dorsal hippocampus in consolidation of object recognition memory. *Neurosci.* Lett. 405:142-146

66. Cohen, S. J. *et al.* (2013) The rodent hippocampus is essential for nonspatial object memory. *Curr Biol.* 23: 1685-1690

67. Cheng, J. *et al.* (2014) A role for H3K4 monomethylation in gene repression and partitioning of chromatin readers. *Mol. Cell* 53:979–992

68. Snaidero, N. and Simons, M. (2014) Myelination at a glance. *J of Cell Sci.* 127:2999-3004

69. Jones, A.J. and Rumsby, M.G. (1975) The intrinsic fluorescence characteristics of the myelin basic protein. *J of Neuro Chem*. 25(5):565-572

70. Bertero, A. *et al.* (2015) Activin/nodal signaling and NANOG orchestrate human embryonic stem cell fate decisions by controlling the H3K4me3 chromatin mark. *Genes Dev.* 29:702-717

71. Pérez-Lluch, S. *et al.* (2015) Absence of canonical marks of active chromatin in developmentally regulated genes. *Nat Genet.* 47(10):1158-1167

72. Jiang, H. *et al.* (2013) Regulation of transcription by the MLL2 complex and MLL complex-associated AKAP95. *Nat Struct Mol Biol.* 20:1156-1164

73. Hu, D. *et al.* (2017) Not all H3K4 methylations are created equal: Mll2/COMPASS dependency in primordial germ cell specification. *Mol Cell.* 65:460-475.e6

74. Stein, A. B. *et al.* (2011) Loss of H3K4 methylation destabilizes gene expression patterns and physiological functions in adult murine cardiomyocytes. *J Clin Invest.* 121: 2641-2650

75. Bertero, A. *et al.* (2015) Activin/nodal signalling and NANOG orchestrate human embryonic stem cell fate decisions by controlling the H3K4me3 chromatin mark. *Genes Dev*. 29: 702-717

76. Yan, J. *et al.* (2018) Histone H3 lysine 4 monomethylation modulates long-range chromatin interactions at enhancers. *Cell Research.* 28:204-220

77. Benayoun, B.A. *et al.* (2014) H3K4me3 breadth is linked to cell identity and transcriptional consistency. *Cell.* 158(3):673-688